View metadata, citation and similar papers at core.ac.uk

brought to you by CORE

provided by The University of Utah: J. Willard Marriott Digital Library

FAILURE PROGRESSIONS IN SANDWICH COMPOSITES FOR CRASHWORTHINESS APPLICATIONS

by

James Terry Van Otten

A thesis submitted to the faculty of
The University of Utah
in partial fulfillment of the requirements for the degree of

Master of Science

Department of Mechanical Engineering

The University of Utah

May 2011

Copyright © James Terry Van Otten 2011

All Rights Reserved

The University of Utah Graduate School

STATEMENT OF THESIS APPROVAL

The thesis of **James Terry Van Otten**

has been approved by the following supervisory committee members:

Daniel O. Adams	, Chair	**05/04/2010** Date Approved
K. Larry DeVries	, Member	**05/04/2010** Date Approved
Kenneth L. Monson	, Member	**05/04/2010** Date Approved

and by **Tim A. Ameel**, Chair of the Department of **Mechanical Engineering**

and by Charles A. Wight, Dean of The Graduate School.

ABSTRACT

Sandwich composites are being considered for several automotive applications due to their high strength-to-weight and stiffness-to-weight ratios. Since crashworthiness is an important consideration for automotive applications, energy absorption under impact loading is also a key property. This investigation focused on the effects of material and geometric variables of automotive sandwich composites on failure progressions and energy absorption during edgewise impact loading. The baseline sandwich configurations consisted of woven carbon-epoxy or P4 carbon-epoxy facesheets and either end-grain balsa or polyurethane foam cores. In an effort to explore the feasibility of designing a sandwich composite configuration for energy absorption, variations on facesheet thickness, core thickness, and core density were investigated. By varying each of these parameters, the effects on failure mode and energy absorption could be determined. Results suggest that sandwich composites may be designed for enhanced energy absorption through the proper selection of facesheet and core materials and geometries such that high energy absorbing failure progressions are produced.

To Brydger, Mom, and Dad

TABLE OF CONTENTS

ABSTRACT iii

LIST OF FIGURES vi

LIST OF TABLES ix

ACKNOWLEDGEMENTS x

Chapter

1. DESIGN CONSIDERATIONS FOR ENERGY ABSORPTION IN AUTOMOTIVE SANDWICH COMPOSITES 1

    Abstract 2
    Introduction 2
    Materials 3
    Edgewise Impact Testing 5
    Results and Discussion 7
    Summary and Conclusions 19
    Acknowledgements 20
    References 20

2. PREDICTION OF FAILURE PROGRESSIONS IN SANDWICH COMPOSITES FOR CRASHWORTHINESS APPLICATIONS 21

    Abstract 21
    Introduction 22
    Analytical Model – Elastica Approach 23
    Determining Values for κ_B 34
    Using MATLAB to Solve Analytical Model 36
    Materials 42
    Analytical Model Results 44
    Using ANSYS to Validate κ_B Calculation Method 52
    Summary and Conclusions 56
    Notation 60
    References 62

LIST OF FIGURES

Figure Page

1.1 Edgewise compression drop-weight impact test configuration 5

1.2 Typical force versus displacement plot illustrating the peak force and energy absorbed 6

1.3 Normalized energy absorption results for edgewise drop-weight impact of baseline configurations 7

1.4 Failure progression for Woven Carbon/Balsa baseline specimens....8

1.5 Force versus displacement curves for Woven Carbon/Balsa baseline specimens....8

1.6 Local buckling and facesheet debonding of a Woven Carbon/Polyurethane specimen 9

1.7 Initial facesheet compression failure locations for P4 Carbon/Balsa specimens....9

1.8 Force versus displacement curves for P4 Carbon/Balsa baseline specimens 10

1.9 P4 Carbon/Polyurethane specimen 2 exhibiting facesheet failure with subsequent debonding and buckling....10

1.10 Normalized energy absorption results for edgewise drop-weight impact of core density variation configurations 12

1.11 Woven Carbon/High Density Polyurethane (WC-HDPU) specimen 2 exhibiting debonding/buckling 12

1.12 Normalized energy absorption results for edgewise drop-weight impact of core thickness variation configurations....13

1.13 P4-B-.2core specimen 1 exhibiting middle facesheet compression/buckling and low energy absorption....14

1.14 P4-B-.3core specimen 1 exhibiting facesheet compression/crushing and increased energy absorption....14

1.15 P4-PU-.2core specimen 1 exhibiting facesheet compression/buckling....15

1.16 P4-PU-.3core specimen 2 exhibiting facesheet compression/reloading....15

1.17 P4-PU-.4core specimen 1 exhibiting facesheet compression/reloading....16

1.18 Normalized energy absorption results for edgewise drop-weight impact of facesheet thickness variation configurations....17

1.19 2-ply Woven Carbon/Balsa specimen 1 exhibiting facesheet compression/reloading....17

1.20 4-ply Woven Carbon/Balsa specimen 1 exhibiting progressive crushing....18

1.21 8-ply Woven Carbon/Balsa specimen 2 experiencing progressive facesheet compression failures....18

1.22 2-ply Woven Carbon/Polyurethane specimen 1 exhibiting local facesheet debonding/buckling and low energy absorption....19

1.23 8-ply Woven Carbon/Polyurethane specimen 1 exhibiting buckling/facesheet compression....19

2.1 Adaptation of (a.) a general sandwich composite to (b.) the Elastica approach....24

2.2 Illustration of (a.) facesheet fracture and (b.) core/facesheet debond growth....26

2.3 Adaptation of a general sandwich composite (a.) to a Beam on Elastic Foundation (b.)....35

2.4 Depiction of three energy states used in MATLAB solution of analytical model....38

2.5 Flow chart outlining general MATLAB procedure....40

2.6 Plot of h_{trans} as a function of E_c and t_c....46

2.7 Plot of h_{trans} as a function of G_{Ic} and t_c....48

2.8 Plot of h_{trans} as a function of E_{fs} and t_{fs}....50

2.9 Facesheet stress versus crack length for variation of facesheet thickness 51

2.10 Representation of a typical mesh used in ANSYS.....53

2.11 Progressive zooming of mesh showing dimensions used in calculation 55

2.12 Finite element mesh showing dimensions for calculation of $M_{cracktip}$.....55

LIST OF TABLES

Table Page

1.1 Summary of four sandwich configuration materials/manufacturing methods.....5

2.1 Material properties used with ANSYS 53

2.2 Comparison of ANSYS and BOEF calculations for κ_B 57

ACKNOWLEDGEMENTS

I would like to thank Dr. Dan Adams, my advisor and supervisory chair, for his expertise, guidance, and for reminding me that research papers should always tell a great story. I would also like to thank Dr. Larry DeVries and Dr. Ken Monson for their time given as members of my supervisory committee.

I would like to thank the members of the Automotive Composites Consortium (ACC) for their financial support and guidance.

I would like to thank my predecessors Austin Van Otten, Nick Ellerbeck, and Scott Stapleton for teaching me practical composites knowledge and laying a solid foundation upon which this research was performed.

Most of all, I would like to thank my family and especially my wife, Brydger, for giving me the love and support I needed to achieve my goals. I could not have done it without you all.

CHAPTER 1

DESIGN CONSIDERATIONS FOR ENERGY ABSORPTION IN AUTOMOTIVE SANDWICH COMPOSITES

James Van Otten, Scott E. Stapleton, Daniel O. Adams
Department of Mechanical Engineering
University of Utah
Salt Lake City, Utah 84112

Published In:
Proceedings of the 40th International SAMPE Technical Conference
2008, Memphis, TN

DESIGN CONSIDERATIONS FOR ENERGY ABSORPTION IN AUTOMOTIVE SANDWICH COMPOSITES

James Van Otten, Scott E. Stapleton, and Daniel O. Adams
Department of Mechanical Engineering
University of Utah
Salt Lake City, UT 84112

ABSTRACT

Sandwich composites are being considered for several automotive applications due to their high strength-to-weight and stiffness-to-weight ratios. Since crashworthiness is an important consideration for automotive applications, energy absorption under impact loading is also a key property. This investigation focused on the effects of material and geometric variables of automotive sandwich composites on failure progressions and energy absorption during edgewise impact loading. The baseline sandwich configurations consisted of woven carbon-epoxy or P4 carbon-epoxy facesheets and either end-grain balsa or polyurethane foam cores. In an effort to explore the feasibility of designing a sandwich composite configuration for energy absorption, variations on facesheet thickness, core thickness, and core density were investigated. By varying each of these parameters, the effects on failure mode and energy absorption could be determined. Results suggest that sandwich composites may be designed for enhanced energy absorption through the proper selection of facesheet and core materials and geometries such that high energy absorbing failure progressions are produced.

KEY WORDS: Sandwich Structures, Energy Absorption, Applications-Automotive

1. INTRODUCTION

One of the major design considerations within the automotive industry is crashworthiness. Thus for fiber reinforced composites to be utilized in many automotive applications, they must exhibit a sufficient degree of crashworthiness. The Composite Materials Handbook (CMH-17) describes the objective of designing for crashworthiness to "eliminate injuries and fatalities in relatively mild impacts, and to minimize them in all severe collisions [1]." To date, much of the research to investigate composite crashworthiness has focused on monolithic composites with either glass or carbon fiber reinforcements. However, a more recent interest in using sandwich composites for roof and floor applications has led to an interest in exploring the crashworthiness of sandwich composites.

For this purpose, a research investigation was initiated to investigate the energy absorption characteristics of composite sandwich structures under crush loading. The first phase of this project investigated a total of 13 different sandwich configurations of comparable weight and thickness. Mechanical testing was performed to investigate facesheet/core compatibility issues and sandwich performance under flexure and edgewise compression loading. Results of this initial evaluation phase are presented elsewhere [2, 3]. In the second phase of the project, four top-performing sandwich configurations were selected for further evaluation. The energy absorption and initial failure mechanisms and failure progressions of these four selected sandwich configurations were evaluated under both quasi-static and dynamic edgewise compression loading in order to determine high energy-absorbing mechanisms/progressions. Results of this second phase are available in reference [4].

In the third phase of this research project, further research was performed using the same four top-performing sandwich configurations evaluated during the second phase. Based on previous findings, variations in energy absorption associated with three sandwich composite parameters were investigated; the three parameters considered were core density, core thickness, and facesheet thickness. Energy absorption was evaluated under dynamic edgewise compression loading using drop-weight impact testing. Emphasis was placed on evaluating changes in initial failure mechanisms, failure progressions, and energy absorption resulting from each parameter. Knowledge of the initial failure mechanisms and failure progressions leading to high energy absorption is believed to be a key step in the development of crashworthy sandwich composite structures for automotive applications.

2. MATERIALS

2.1. Facesheet/Core Materials

All four sandwich configurations investigated were fabricated at the University of Utah. Table 1 summarizes the materials and manufacturing methods used for these four configurations. The sandwich configurations with woven carbon facesheets consisted of a T300B 3K plain weave carbon fabric. The two sandwich configurations with P4 carbon facesheets used a carbon random mat made by the Powder Programmable Preforming Process (P4). Both types of carbon fiber preforms were infiltrated with EPON 862 epoxy resin and EPON 9553 hardener [5]. The core materials included polyurethane foam and end-grain balsa wood. The polyurethane foams, with densities of 160 and 320 kg/m^3 were supplied by General Plastics Manufacturing Company [6]. The end-grain balsa woods, with densities of 97, 112, and 256 kg/m^3 were supplied by Baltek Corporation [7].

The two sandwich configurations with woven carbon/epoxy facesheets were fabricated using a single-step Vacuum Assisted Resin Transfer Molding (VARTM) process. A quasi-isotropic $[(0/90)/(\pm 45)]_{3T}$ lay-up of plain weave fabric was placed on both sides of the core material. The sandwich panel was wrapped in a layer of porous Teflon-coated fiberglass followed by a resin transfer medium (plastic mesh). The assembly was placed on a flat metal plate and vacuum bagged. Once the vacuum bag was sealed, a vacuum pump was used to pull the resin through an inlet tube. Following complete infiltration of the carbon fabric facesheets, the panel was cured under vacuum for two hours at 50°C.

Table 1. Summary of four sandwich configuration materials/manufacturing methods.

Sandwich Configuration	Facesheet Material	Core Material	Manufacturing Method
Woven Carbon/Balsa WC-B	Woven carbon fabric/epoxy	Balsa	One-step VARTM
Woven Carbon/Polyurethane WC-PU	Woven carbon fabric/epoxy	Polyurethane	One-step VARTM
P4/Balsa P4-B	Random carbon mat (P4)/epoxy	Balsa	Two-step VARTM
P4/Polyurethane P4-PU	Random carbon mat (P4)/epoxy	Polyurethane	Two-step VARTM

A two-step VARTM method was used to fabricate the P4 facesheet configurations. The sandwich was placed between two flat acrylic plates, which served as a mold. Acrylic was selected for the mold material such that resin infiltration could be visually monitored. After wet-out of the facesheets, additional pressure was applied to the panel to reduce the facesheet thickness by placing the vacuum-bagged assembly into a heated press. A pressure of 1.0 MPa was selected for use based on the compressive strength of the core material and the required pressure to obtain a facesheet thickness comparable to the woven carbon facesheets. Pressure was applied for two hours while the temperature of the platens was held at 50°C. Vacuum was maintained on the bagged assembly throughout the cure process.

2.2. Description of Sandwich Parameter Variations

Three sandwich parameters were investigated: core density, core thickness and facesheet thickness. Variations in each of these three sandwich parameters are described below.

2.2.1. Core Density

By varying the density of the two core materials used in the sandwich constructions, the strength and stiffness of the core is varied. Additionally, the strength of the core/facesheet bond is affected by the core density. Thus, changes in the initial failure mode and failure progression are possible. Increasing core density was expected to produce high energy-absorbing failures if the initial load required to debond the facesheets from the core could be elevated to a level that exceeds the load required to fail the facesheet in compression.

2.2.2. Core Thickness

By varying the thickness of the sandwich core, the moment of inertia for the sandwich composite can be tailored to prevent buckling and induce facesheet compression failure. A thicker core places the facesheets further from the neutral axis, increasing the load required for buckling, and promoting facesheet compression failure as the initial failure mode, which is desired for increased energy absorption. For both core materials considered, core thicknesses of 5 mm (0.2 in.), 8 mm (0.3 in.), 10 mm (0.4 in.), and 13 mm (0.5 in.) were used.

2.2.3. Facesheet Thickness

Facesheet thickness, like core thickness, affects the moment of inertia of the sandwich composite as well as the bending stiffness of the individual facesheets themselves. Although thicker facesheets may resist global buckling, they are more prone to delaminate from the core prior to facesheet failure under edgewise compression loading. In this investigation, woven carbon/epoxy facesheets of thickness 4 ply, 6 ply, and 8 ply were used. The P4 carbon/epoxy facesheets were used in thicknesses of 1 and 2 ply.

3. EDGEWISE IMPACT TESTING

Drop weight testing was used to assess the edgewise compression performance of the four sandwich configurations under dynamic loading. The test configuration used for edgewise drop-weight impact testing was a modified form of ASTM C 364 [8] and is shown in Figure 1. The crosshead of the impact tower had a mass of 46.6 kg and the fixture above the force link had a mass of 10.0 kg. Vertical alignment of the crosshead was maintained using vertical guide rods and linear ball bearings. Springs and metal stoppers were used to keep the top fixture from contacting the bottom fixture during impacting. The required drop height for each sandwich configuration was determined based on the amount of energy absorbed in quasi-static edgewise compression testing. The drop heights ranged from 1.2 to 3.0 meters, producing initial crosshead velocities between 4.4 and 6.9 m/s.

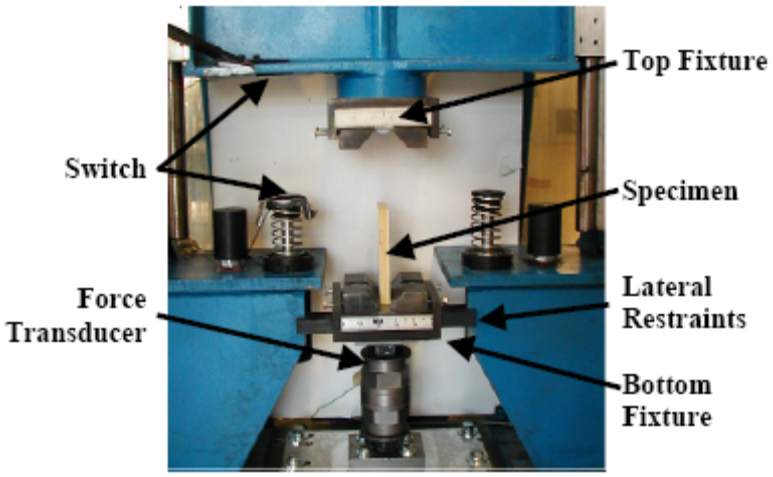

Figure 1. Edgewise compression drop-weight impact test configuration.

The energy absorption, peak load, and failure progression were determined for each sandwich specimen tested. Energy absorption was recorded over a 51 mm crush length. A Kistler 9372A quartz force link was affixed between the lower fixture and the tower base to provide force versus time data. The charge output of the force link was converted into a proportionally controlled voltage using a Kistler 5010B charge amplifier. Data was collected at a sampling rate

of 50 kHz using National Instruments LabVIEW 7.1 [9] with no filtering. The software scaled the data and provided a force versus time history of the impact event. Numerical integration techniques were employed to obtain velocity and displacement responses. A force versus displacement plot was generated for each test and numerically integrated to obtain the total energy absorption. A manual switch located on the crosshead and the top of the damping spring was used to signal the end of the specimen crush length such that the springs and stoppers were not included in the impact event. A high-speed camera was used to capture the impact event at 2,000 frames per second.

Failure progression, peak force, and weight-normalized energy absorption were determined for each specimen tested. Peak force was defined as the highest force seen in the force versus displacement plot (Figure 2). Energy absorption was found by calculating the area below the force vs. displacement curve as shown in Figure 2. Because weight savings is a primary concern for automotive sandwich structures, the energy absorbed was reported in a weight-based normalized form, energy per areal weight. The areal weight, or weight per unit surface area, was calculated as

$$AW = \frac{w}{bh}, \tag{1}$$

where

AW = areal weight (kg/m^2)
w = specimen weight (kg)
b = specimen width (m)
h = specimen height (m).

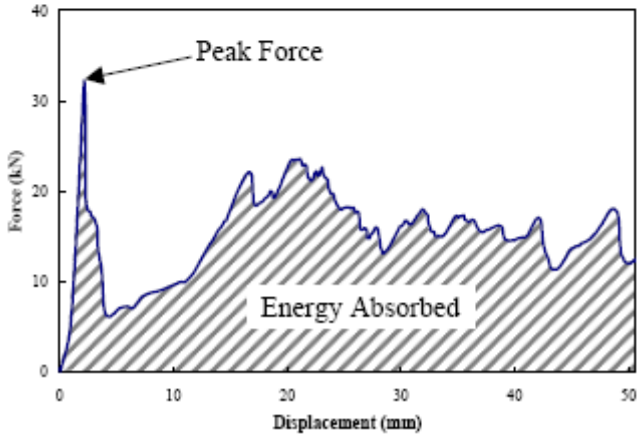

Figure 2. Typical force versus displacement plot illustrating the peak force and energy absorbed.

4. RESULTS AND DISCUSSION

4.1. Baseline Sandwich Configurations

Figure 3 shows the normalized energy absorption obtained for each of three specimens of the four baseline sandwich configurations listed in Table 1. All baseline sandwich configurations had core thicknesses of approximately 13 mm. For the Woven Carbon/Balsa configuration, specimens 1 and 3 failed by facesheet curling followed by buckling as shown in Figure 4a. Although the facesheet curling failure mode is favorable for energy absorption, the subsequent buckling absorbed little energy. Specimen 2 failed due to a facesheet compression failure about 15 mm from the top of the specimen (Figure 4b). Even though the facesheets in this specimen did not experience curling, the specimen continued to reload and crushed progressively, absorbing nearly the same amount of energy as the other two specimens (1 and 3) from this configuration. Force versus displacement curves from each type of failure progression are shown in Figure 5.

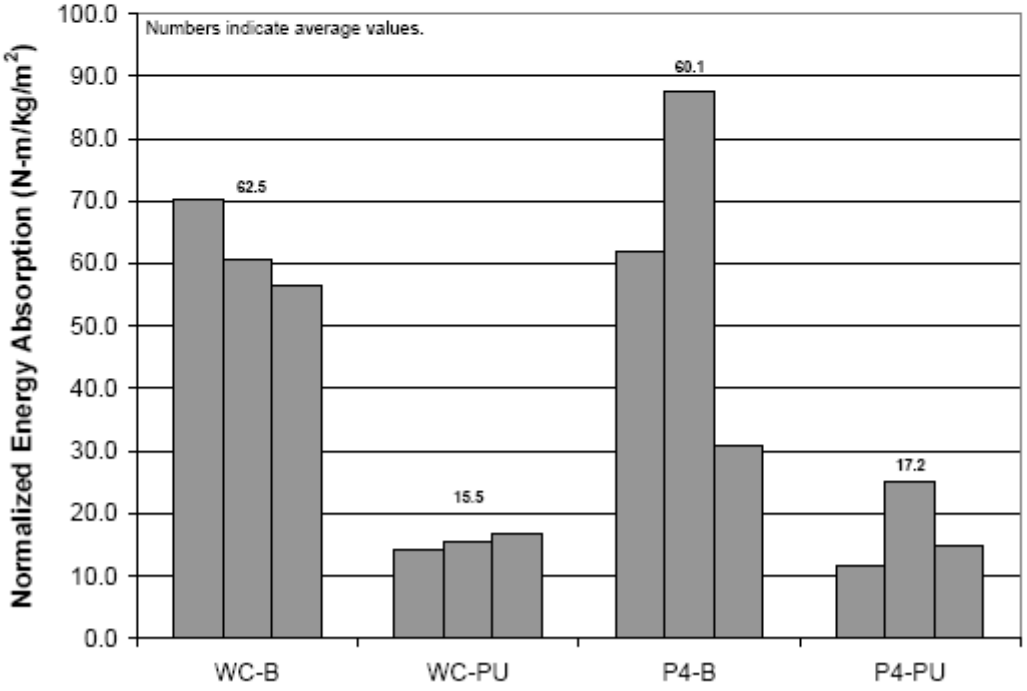

Figure 3. Normalized energy absorption results for edgewise drop-weight impact of baseline configurations.

a. Facesheet curling b. Facesheet compression failure

Figure 4. Failure progression for Woven Carbon/Balsa baseline specimens.

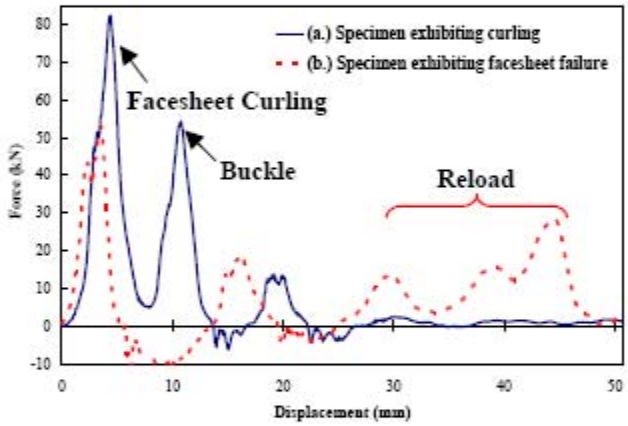

Figure 5. Force versus displacement curves for Woven Carbon/Balsa baseline specimens.

For the Woven Carbon/Polyurethane configuration, all three baseline specimens tested experienced similar failures, as the facesheets buckled outward in an opposing manner as shown in Figure 6. This facesheet buckling occurred near the top of the specimen producing a facesheet debond which propagated along the entire length of the specimen. As a result of these debonds, energy absorption for this baseline configuration was well below that measured in the Woven Carbon/Balsa baseline configuration.

Failure progressions observed in the P4 Carbon/Balsa specimens indicated that the location of the initial facesheet compression failures and the resulting specimen alignment are pivotal for energy absorption. Specimen 2, the highest energy absorber, failed near the bottom of the specimen (Figure 7a) and remained aligned during subsequent loading. The other two specimens (1 and 3) failed away from the specimen ends (Figure 7b). Specimen 1 realigned later in the impact event, while Specimen 3 failed to reload to a significant level. Force versus displacement curves from each type of failure progression are shown in Figure 8.

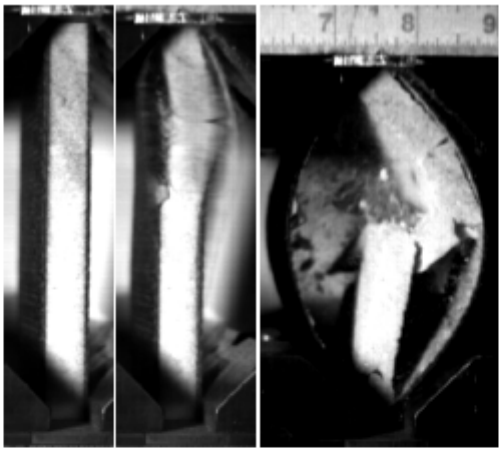

Figure 6. Local buckling and facesheet debonding of a Woven Carbon/Polyurethane specimen.

a. Failure at bottom of specimen. b. Failure away from specimen ends.

Figure 7. Initial facesheet compression failure locations for P4 Carbon/Balsa specimens.

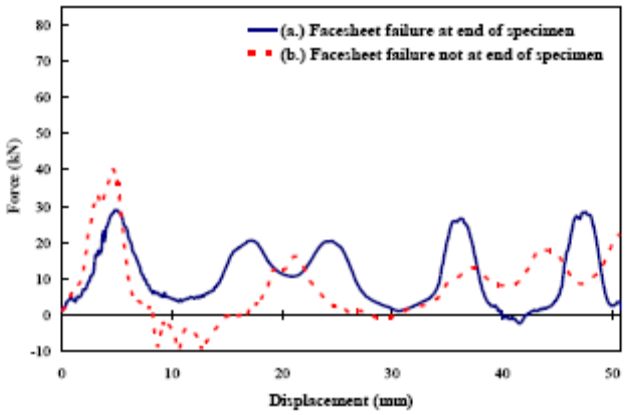

Figure 8. Force versus displacement curves for P4 Carbon/Balsa baseline specimens.

For the P4 Carbon/Polyurethane configuration, varying failures occurred with subsequent differences in energy absorption. In specimens 1 and 3 both facesheets delaminated from the core producing low energy absorption. In specimen 2, one facesheet failed whereas the other buckled and delaminated away from the core as shown in Figure 9. Additional energy was absorbed by the facesheet that remained attached to the core, making it the highest energy absorbing specimen of the three tested. However, the energy absorption for this baseline configuration was well below that measured in the Woven Carbon/Balsa and P4/Balsa baseline configurations.

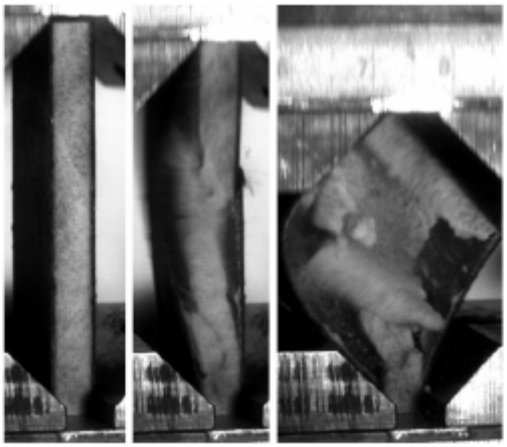

Figure 9. P4 Carbon/Polyurethane specimen 2 exhibiting facesheet failure with subsequent debonding and buckling.

4.2. Effects of Core Density Variations

To investigate the effect of core density on energy absorption, the following core materials were utilized:

- Low density balsa wood, "LDB" (Baltek SuperLite S56, 97 kg/m^3)
- Baseline density balsa wood, "B" (Baltek SuperLite S67, 112 kg/m^3)
- High density balsa wood, "HDB" (Baltek SuperLite 14/15, 256 kg/m^3)
- Baseline density polyurethane foam, "PU" (General Plastics Last-A-Foam FR-6710, 160 kg/m^3)
- High Density Polyurethane foam, "HDPU" (General Plastics Last-A-Foam FR-6720, 320 kg/m^3)

Figure 10 shows the effect of core density variations on the normalized energy absorption from each of the four sandwich configurations listed in Table 1. Results show that for the Woven Carbon/Polyurethane configuration, increasing the core density increased the normalized energy absorption. This result is believed to be due to the increased stiffness of the higher density core better supporting the facesheets. Although the high core density specimens from this sandwich configuration experienced facesheet debonding failures similar to the baseline configuration, the high density core appeared to produce a stronger core/facesheet bond, and thus more energy was required to debond the facesheets. The improved bond also resulted in significantly higher peak loads for the high core density configuration (103 kN versus 51 kN for baseline specimens). This increased energy absorption and peak load is illustrated by specimen 2 (Figure 11), which failed in buckling after the facesheets debonded from the core and buckled away from each other. A similar increase in normalized energy absorption with increasing core density was observed for the P4/Polyurethane configuration. However, no significant increase in normalized energy absorption was observed with increasing core density for either sandwich configuration with the balsa wood core.

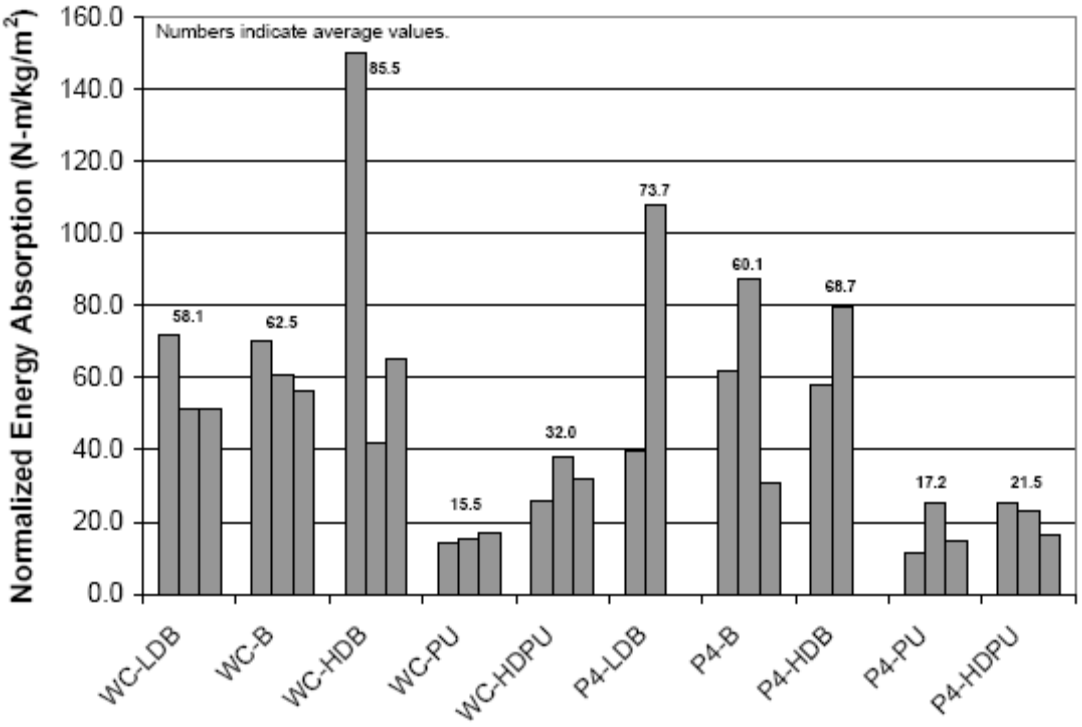

Figure 10. Normalized energy absorption results for edgewise drop-weight impact of core density variation configurations.

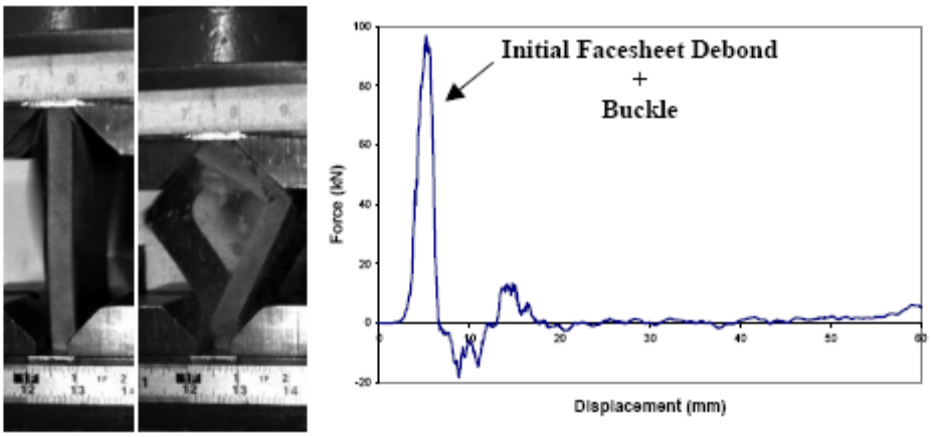

Figure 11. Woven Carbon/High Density Polyurethane (WC-HDPU) specimen 2 exhibiting debonding/buckling.

4.3. Effects of Core Thickness Variations

By changing the core thickness, the moment of inertia for the sandwich composite can be altered without changing the facesheets or the core density. As a result, the resistance to global buckling under edgewise compression loading is increased. For evaluating core thickness effects, sandwich cores with thicknesses of 5 mm (0.2 in.), 8 mm (0.3 in.), 10 mm (0.4 in.) were used in addition to the baseline core thickness of 13 mm (0.5 in.).

Figure 12 shows the effect of core thickness variations on the normalized energy absorption for each of the four sandwich configurations listed in Table 1. Of particular interest are the results from the P4 Carbon/Balsa and P4 Carbon/Polyurethane configurations. Increased normalized energy absorption was observed for the P4 Carbon/Balsa configuration with increasing core thickness, producing the highest normalized energy absorption of the four configurations. All of the P4 Carbon/Balsa specimens appear to have failed initially in facesheet compression, but with highly variable results. The 5 mm (0.2 in.) core thickness specimens experienced subsequent buckling, resulting in low energy absorption as shown in Figure 13. The 8 mm (0.3 in.) and 10 mm (0.4 in.) core thickness specimens experienced subsequent crushing as illustrated in Figure 14. This failure progression resulted in normalized energy absorption values that were similar to the baseline configuration and significantly higher than seen in the 5 mm (0.2 in.) specimens.

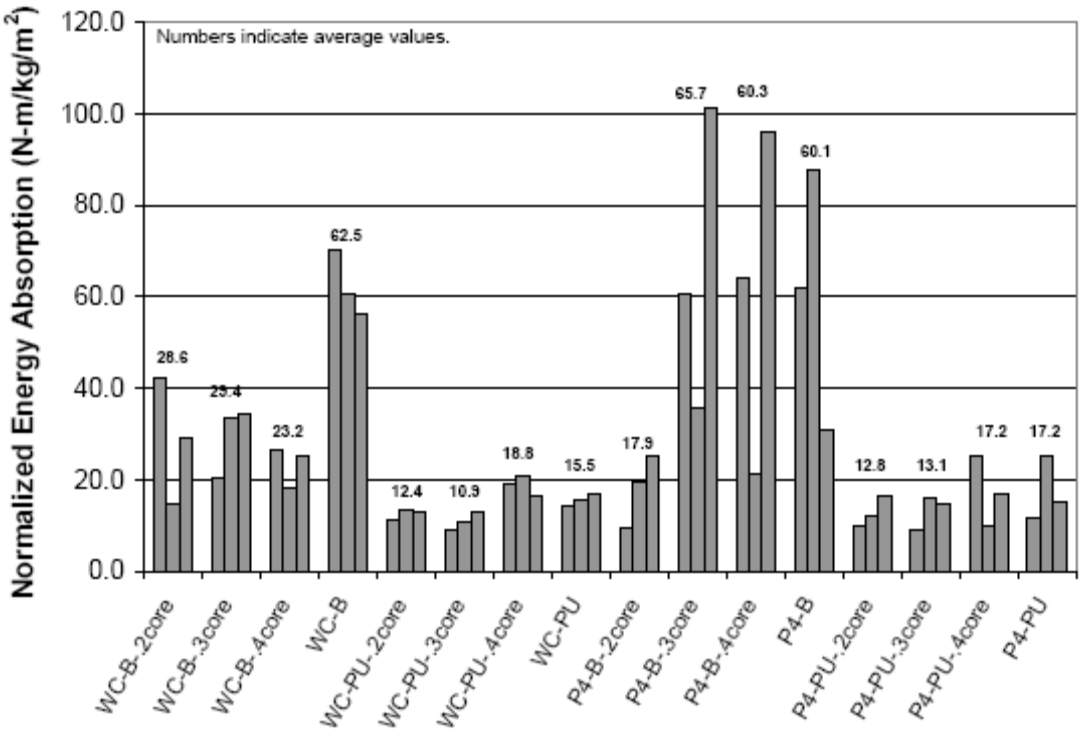

Figure 12. Normalized energy absorption results for edgewise drop-weight impact of core thickness variation configurations.

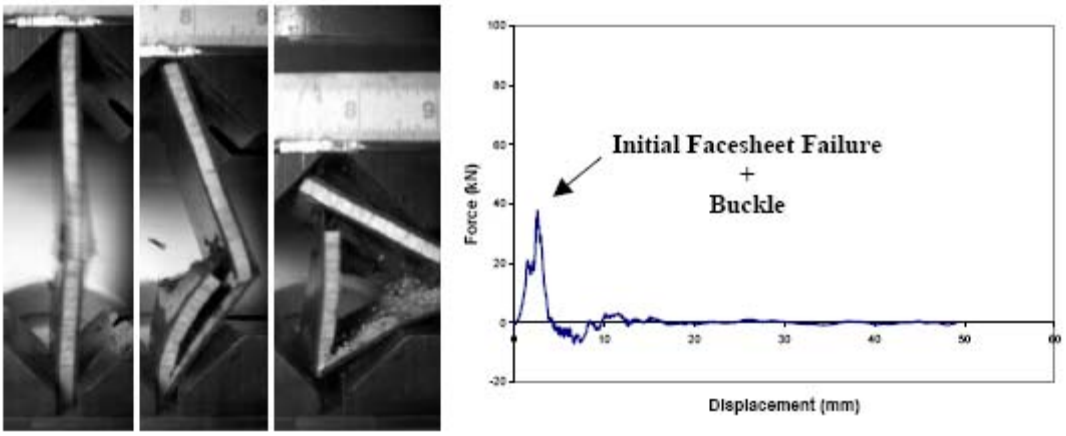

Figure 13. P4-B-.2core specimen 1 exhibiting middle facesheet compression/buckling and low energy absorption.

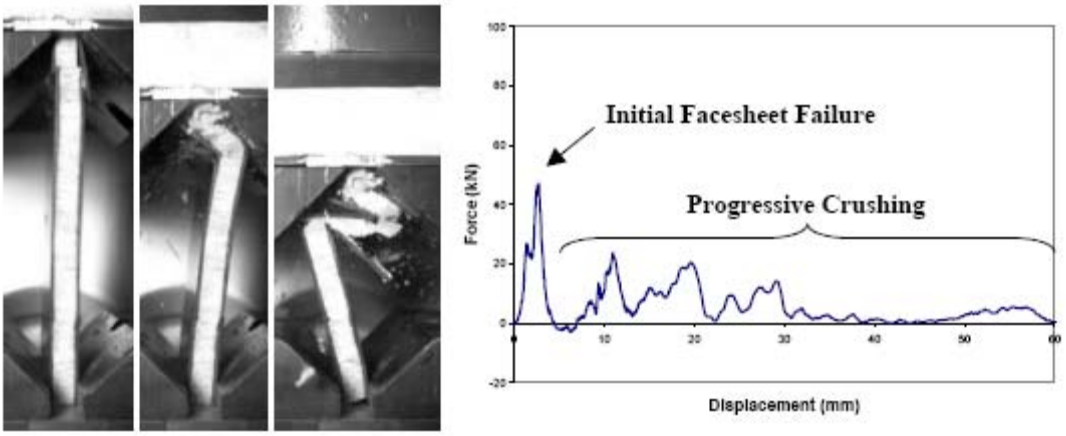

Figure 14. P4-B-.3core specimen 1 exhibiting facesheet compression/crushing and increased energy absorption.

As with the P4 Carbon/Balsa configuration, the P4 Carbon/Polyurethane configuration exhibited an apparent facesheet compression-type failure in each specimen. However, the P4 Carbon/Polyurethane configuration produced lower normalized energy absorption compared to the P4 Carbon/Balsa configuration. This result is believed to be due to the relatively low stiffness of the polyurethane core compared to balsa, which caused post-failure buckling in all of the 5 mm (0.2 in.) thick core specimens (Figure 15). Energy absorption increased slightly as core thickness increased. The 8 mm (0.3 in.) core specimens (Figure 16) absorbed slightly more

energy than the 5 mm (0.2 in.) cores, whereas the 10 mm (0.4 in.) core specimens (Figure 17) experienced higher peak loads and similar reloading to the 8 mm core specimens, resulting in energy absorption values similar to the baseline configuration.

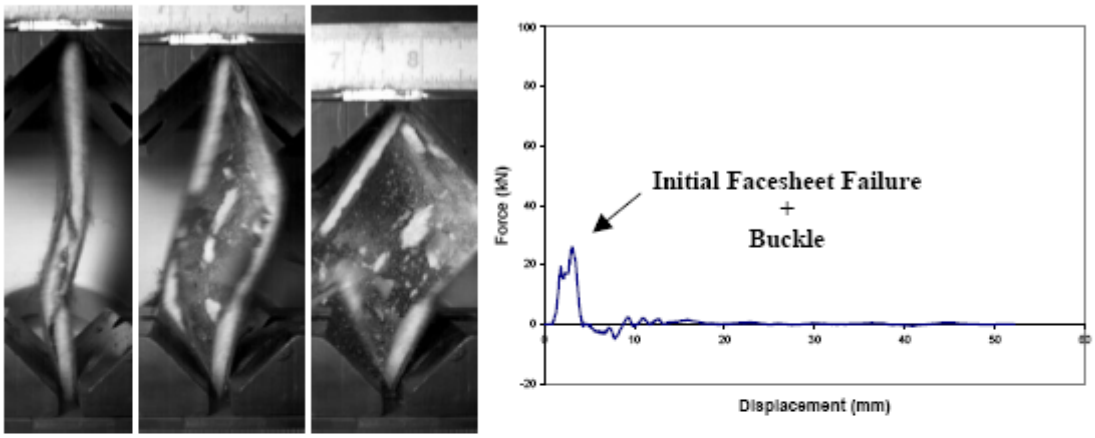

Figure 15. P4-PU-.2core specimen 1 exhibiting facesheet compression/buckling.

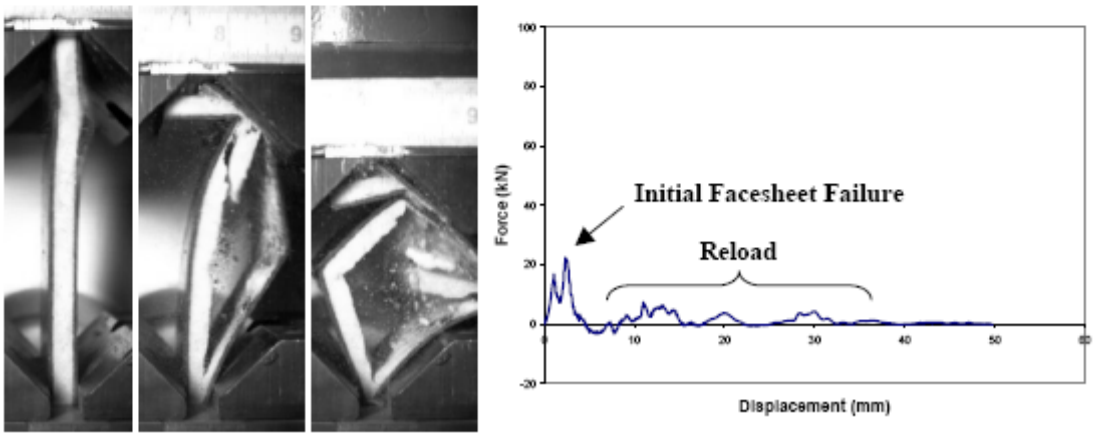

Figure 16. P4-PU-.3core specimen 2 exhibiting facesheet compression/reloading.

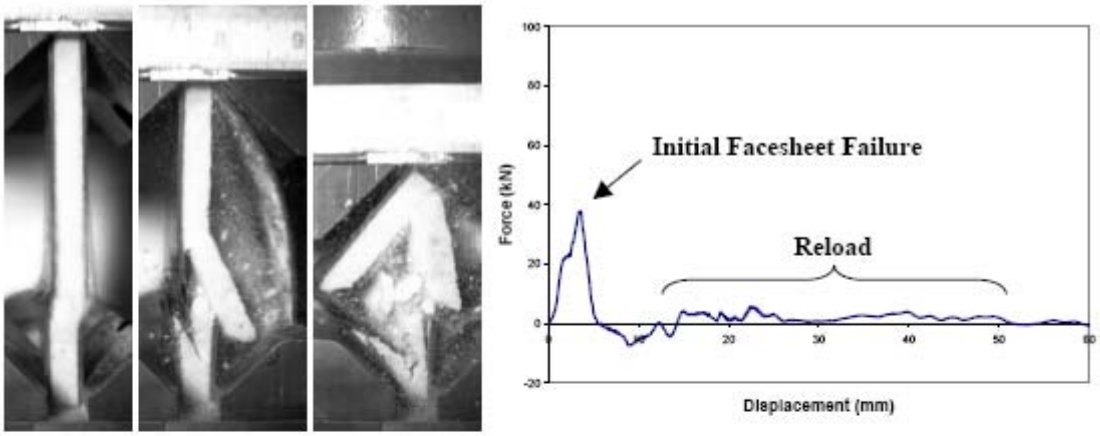

Figure 17. P4-PU-.4core specimen 1 exhibiting facesheet compression/reloading.

4.3. Effects of Facesheet Thickness Variations

Variations in facesheet thickness were explored for both the woven carbon/epoxy and the P4 carbon/epoxy facesheets. Woven carbon/epoxy facesheet thicknesses of 2 ply, 4 ply, 6 ply, (baseline), and 8 ply were investigated. P4 facesheet thicknesses used were 1 ply (baseline) and 2 ply.

Figure 18 shows the effect of facesheet thickness variations on the normalized energy absorption for each of the four sandwich configurations listed in Table 1. Of particular interest are the results from the Woven Carbon/Balsa and Woven Carbon/Polyurethane configurations. The Woven Carbon/Balsa configuration produced the highest normalized energy absorption values for the intermediate thickness (4-ply) facesheets. The thinnest facesheet (2-ply) specimens experienced apparent facesheet compression failures with varying degrees of reloading/crushing as shown in Figure 19. The intermediate thickness (4-ply) facesheet specimens exhibited the highest energy absorption due to repeated reloading during the progressive crushing (Figure 20). As the facesheet thickness increased to 8 plies, however, the normalized energy absorption decreased as less progressive crushing was produced. (Figure 21).

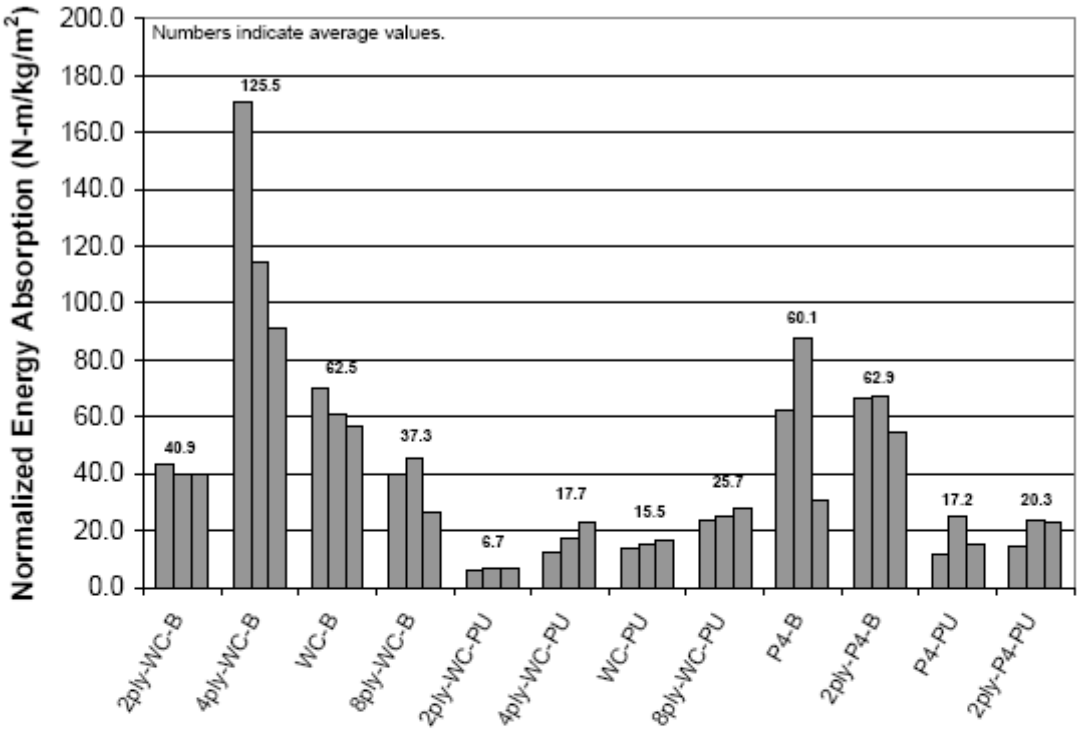

Figure 18. Normalized energy absorption results for edgewise drop-weight impact of facesheet thickness variation configurations.

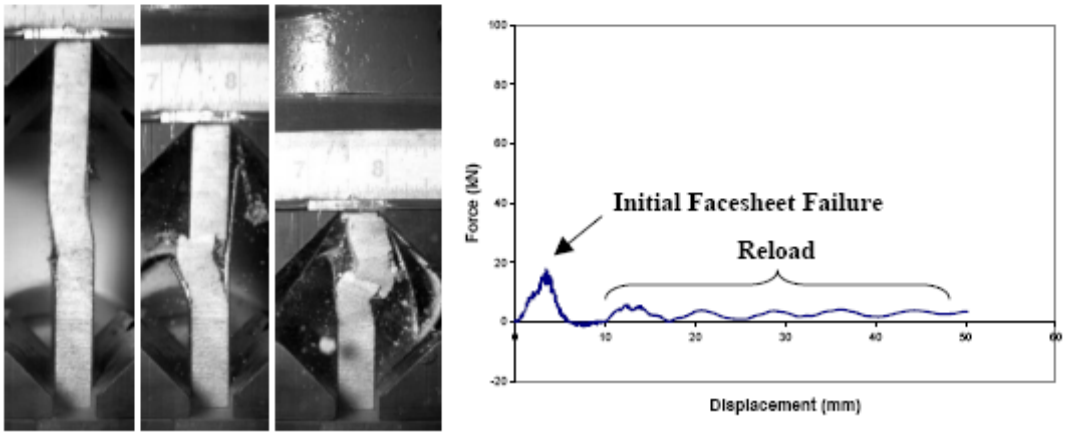

Figure 19. 2-ply Woven Carbon/Balsa specimen 1 exhibiting facesheet compression/reloading.

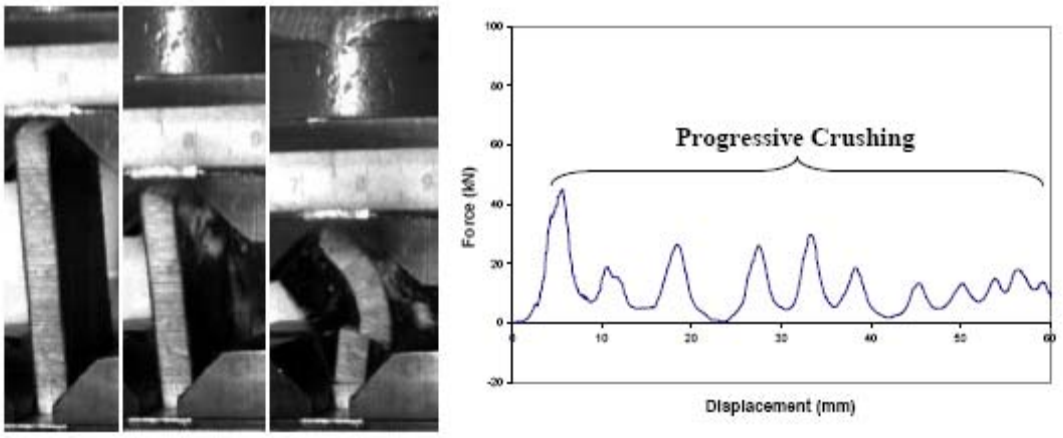

Figure 20. 4-ply Woven Carbon/Balsa specimen 1 exhibiting progressive crushing.

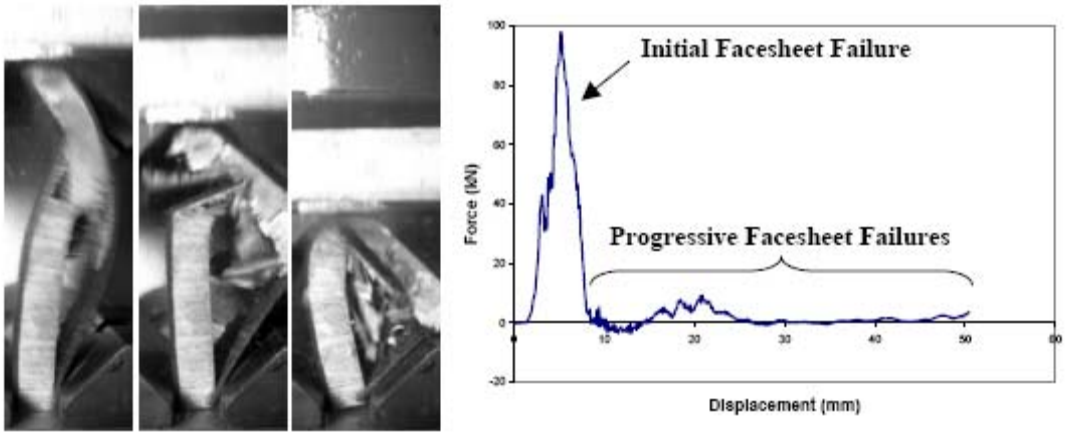

Figure 21. 8-ply Woven Carbon/Balsa specimen 2 experiencing progressive facesheet compression failures.

For the Woven Carbon/Polyurethane configuration, energy absorption increased with increasing facesheet thickness. Both the 2-ply and 4-ply configurations appear to have experienced local facesheet debonding leading to buckling (represented in Figure 22). This debonding is believed to be due to the reduced bending stiffness of the thinner facesheets, which allowed the facesheet to buckle locally and debond from the core. The initial failures occurring in the 8-ply specimens were difficult to determine; high-speed video showed global buckling and facesheet compression occurring virtually simultaneously (Figure 23). However, it is believed that as the facesheet thickness was increased to 8 plies, the facesheets did not experience buckling as observed in the 2-ply and 4-ply facesheet configurations. Rather, it appears that the 8-ply sandwich specimens may have experienced global buckling, leading to shear failures in the foam core, and subsequent facesheet compression failures at these locations. These facesheet compression failures and subsequent specimen reloading resulted in increased energy absorption.

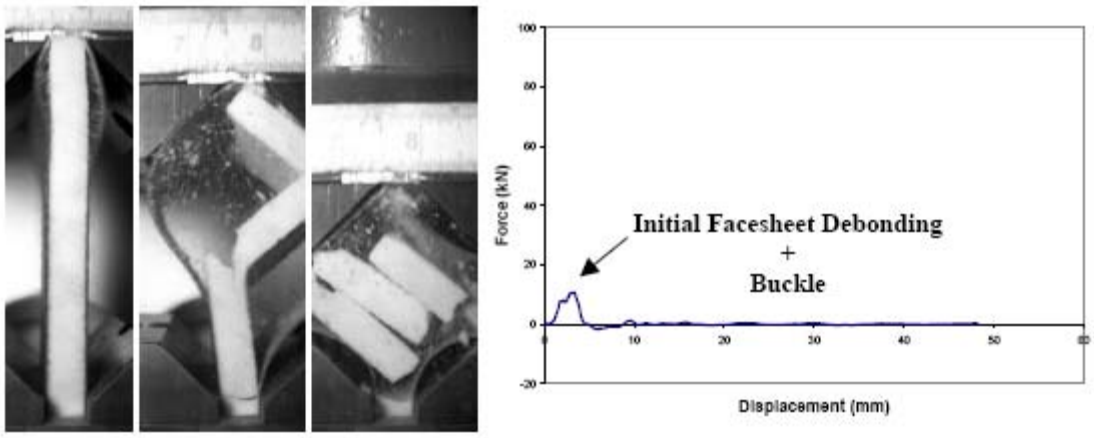

Figure 22. 2-ply Woven Carbon/Polyurethane specimen 1 exhibiting local facesheet debonding/buckling and low energy absorption.

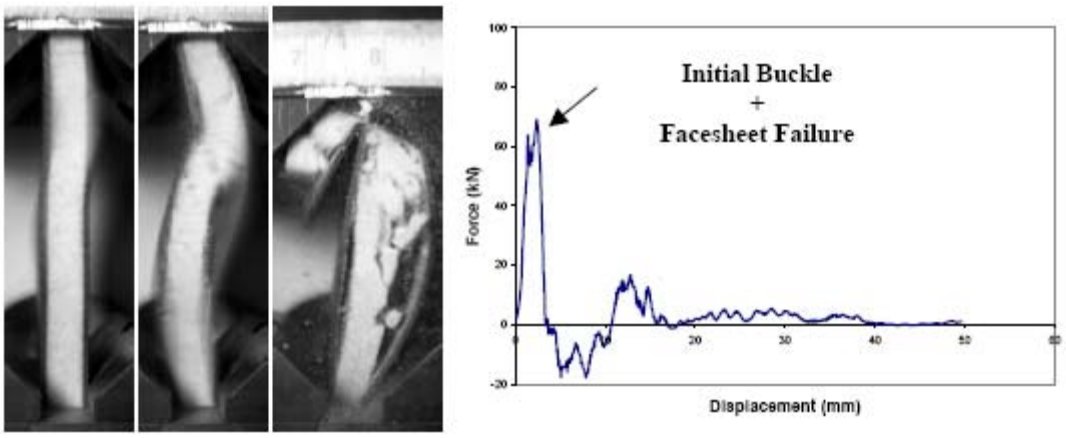

Figure 23. 8-ply Woven Carbon/Polyurethane specimen 1 exhibiting buckling/facesheet compression.

5. SUMMARY AND CONCLUSIONS

Edgewise impact testing was performed using four sandwich configurations that incorporated varying core densities, core thicknesses, and facesheet thicknesses. Of particular interest were changes in the progression of failure and the corresponding energy absorption resulting from these variations. Results showed that energy absorption could be significantly improved with changes in these three parameters, although the apparent initial failure mechanisms did not change for many of the variations investigated. The greatest effect due to changes in core density was observed in the Woven Carbon/Polyurethane configuration, in which the higher density core material appeared to produce a stronger facesheet/core bond and resulted in a greater resistance to facesheet debonding. Energy absorption was found to increase

with increasing core thickness for the P4 Carbon/Balsa and P4 Carbon/Polyurethane sandwich configurations. This effect is believed to be due to increased specimen stability after initial facesheet compression failure with increased core thickness. Finally, energy absorption was found to not increase consistently with increases in facesheet thickness. Rather, an optimal facesheet thickness appeared to exist for energy absorption, especially for the Woven Carbon/Balsa configuration. This finding suggests that although the use of greater thickness facesheets may produce a sandwich composite with higher flexural stiffness and strength, they do not necessarily result in higher energy absorption under edgewise impact loading. Further, the results of this investigation suggest that a sandwich composite may be designed for enhanced energy absorption through the proper selection of facesheet and core materials and geometries such that high energy absorbing failure progressions are produced.

6. ACKNOWLEDGEMENTS

The authors are grateful for the financial sponsorship of the Energy Management Working Group of the Automotive Composites Consortium. The authors acknowledge that this work was supported by the U.S. Department of Energy under cooperative agreement number DE-FC05-95OR22363. Special thanks are extended to Dr. Chaitra Nailadi and Dr. Khaled Shahwan, Technical Monitors, Chrysler Corporation, for their technical guidance and support.

7. REFERENCES

1. "Crashworthiness and Energy Management", Composite Materials Handbook CMH-17-3F, Vol. 3, Ch. 14.
2. Van Otten, A. L., Ellerbeck, N. S., Adams, D. O., Nailadi, C., and Shahwan, K., "Evaluation of Sandwich Composites for Automotive Applications," Proceedings of the 49th International SAMPE Symposium, Long Beach, CA, May 6-10, 2004.
3. Van Otten, A. L., Ellerbeck, N. S., Adams, D. O., and Nailadi, C., "Static and Dynamic Characterization of Sandwich Composites for Automotive Applications,"" Proceedings of the 21st Technical Conference of the American Society of Composites, Dearborn, MI, September 17-20, 2006.
4. Stapleton, S. E., Adams, D. O., and Nailadi, C., "Edgewise Impact Testing of Automotive Sandwich Composites," Proceedings of the 52nd International SAMPE Symposium, Baltimore, MD, June 3-7, 2007.
5. BPF 862 Epon Resin, RSC 9553 curing agent, E.V. Roberts Corporation, Carson, CA.
6. LAST-A-FOAM Polyurethane Foam, General Plastics Manufacturing Company, Tacoma, WA.
7. End-Grain Balsa Wood, Alcan Baltek Corporation, Northvale, NJ.
8. ASTM C 364, "Standard Test Method for Edgewise Compressive Strength of Sandwich Constructions," ASTM International, 2000.
9. LabVIEW 7.1, National Instruments Corporation, Austin, TX.

CHAPTER 2

PREDICTION OF FAILURE PROGRESSIONS IN SANDWICH COMPOSITES FOR CRASHWORTHINESS APPLICATIONS

Abstract

Sandwich composites are being considered for several automotive applications due to their high strength-to-weight and stiffness-to-weight ratios. Since crashworthiness is an important consideration for automotive applications, energy absorption under impact loading is also a key property. This investigation focused on the effects of material and geometric variables of automotive sandwich composites on failure progressions and energy absorption during edgewise impact loading. The baseline sandwich configurations consisted of woven carbon-epoxy or P4 carbon-epoxy facesheets and either end-grain balsa or polyurethane foam cores. In an effort to explore the feasibility of designing a sandwich composite configuration for energy absorption, variations on facesheet thickness, core thickness, and core density were investigated. By varying each of these parameters, the effects on failure mode and energy absorption could be determined. Results suggest that sandwich composites may be designed for enhanced energy absorption through the proper selection of facesheet and core materials and geometries such that high energy absorbing failure progressions are produced.

Introduction

Sandwich composites are used in a variety of applications today, from automotive to aerospace. A sandwich composite is made up of two relatively thin, stiff facesheets on either side of a relatively thick, compliant core material. The role of the facesheets is to lend stiffness and strength to the structure, whereas the core material separates the facesheets to increase the structure's bending stiffness without adding significant weight. Sandwich composites have recently been investigated for use as floorboards and roof panels in automotive applications with a focus on crashworthiness [1]. For automotive applications a crashworthy structure is one that prevents/minimizes injury to occupants during a collision; this is accomplished by designing the structure to maximize energy absorption during a collision.

Through previous studies, sandwich composites under edgewise compression loading were observed to fail under various failure modes, with high and low energy absorbing modes typically being crushing/progressive facesheet fractures and core/facesheet debonding, respectively [1]. Thus, in order to maximize energy absorption it is necessary to design toward facesheet fractures and away from core/facesheet debond. In the current study two competing failure modes were investigated for sandwich composites with a preexisting core/facesheet debond: facesheet fracture and core/facesheet debond growth. An analytical model was developed and used to find the "transition crack length" (h_{trans}), defined as the crack length where the predicted failure mode switches from facesheet fracture to core/facesheet debond growth with increasing crack length. Analyses were performed with several different sets of material properties/sandwich geometries and the results were used to construct plots showing the

variation of h_{trans} with properties of interest. Using these plots, sandwich composites can be tailored to produce facesheet fractures and increased energy absorption.

Analytical Model – Elastica Approach

In order to predict crack growth versus facesheet fracture in sandwich composites with a core/facesheet debond, the Elastica theory was utilized following previous research performed by Aristizabal-Ochoa [2] to calculate large deflections in buckled beam-columns. Once the deflected shape of the beam-column is known, the associated forces and moments can be calculated and the beam-column can be analyzed to predict whether facesheet fracture or crack growth has occurred. The methods used to obtain this solution are described in more detail below.

The adaptation of a general sandwich composite to the Elastica approach is shown in Figure 2.1. The sandwich composite is first identified as symmetric about the core's midplane, and only one-half of the sandwich is analyzed. The beam-column used in the Elastica approach is taken as the debonded section of facesheet, extending from the facesheet tip to the crack tip (points A and B, respectively) with length h. Coordinate system $x'y'$ is oriented such that the x' axis is directed along the line of action of force P_A. For any value of s along the arclength of the beam-column, there exists angle ξ between the tangent to the beam-column and the x' axis.

The Elastica approach calculates deflections in the debonded section of the facesheet, from the facesheet tip to the crack tip. Thus, effects from both the core and the facesheet material in the bonded region of the sandwich composite are neglected. However, because core materials are generally several orders of magnitude more compliant than facesheet materials they act as an elastic foundation for the facesheet,

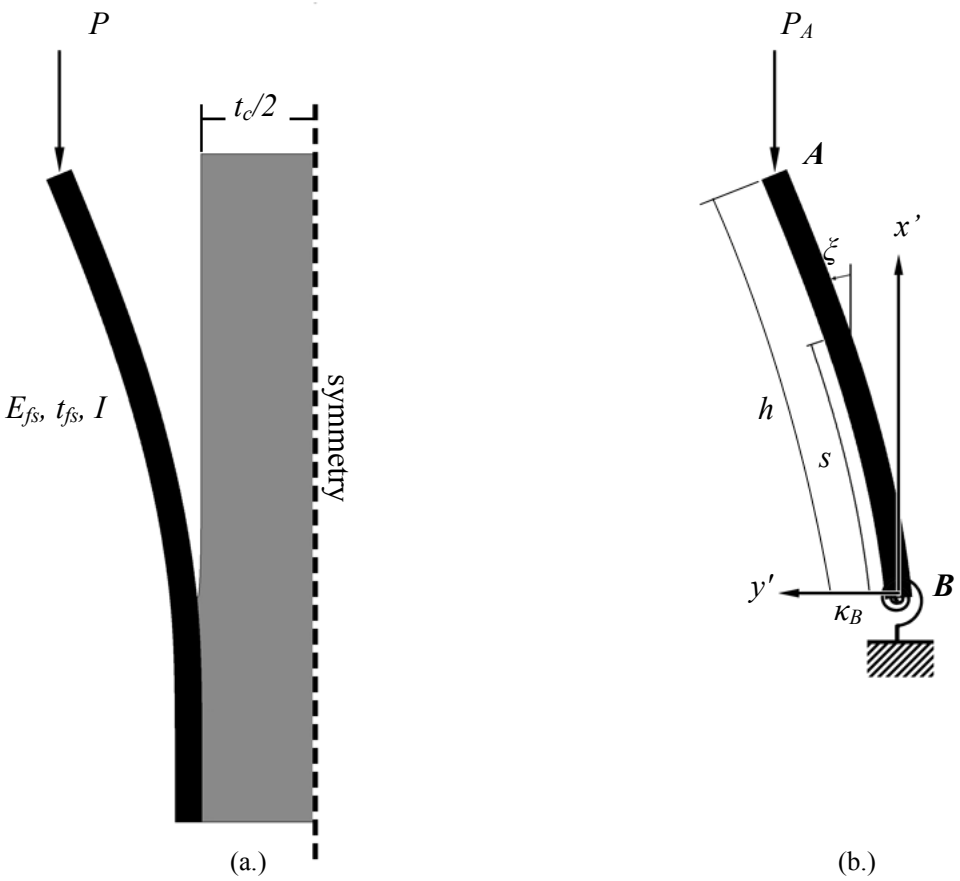

Figure 2.1. Adaptation of (a.) a general sandwich composite to (b.) the Elastica approach

allowing for deflection and rotation at the crack tip. For this reason it was necessary to treat the crack tip as an elastic boundary condition. This was accomplished through the use of a torsional spring of stiffness κ_B at the crack tip, which allows for rotation of the debonded facesheet at the crack tip. Details on the calculation and use of κ_B will be discussed in later sections.

Assumptions

The analytical model discussed in the following sections begins with the assumption that an initial damage event has occurred such that a through-thickness core/facesheet debond exists along both facesheet/core interfaces at one end of the sandwich composite. With this existing debond two modes of failure were considered for use in the analytical model: facesheet fracture and core/facesheet debond growth (illustrated in Figure 2.2).

Both core and facesheet materials are assumed to be linear elastic and homogeneous. The debonded facesheet is treated as an ideal column that is initially straight before load P_A is applied. P_A is applied through the centroid of the beam-column's cross section. Bending is restricted to the *x'y'* plane.

Equation Derivation

Derivation of the equations describing the deflections of the deformed beam-column begins with the governing equation for bending of the beam-column,

$$\frac{d\xi}{ds} = -\frac{M}{E_{fs}I} = \frac{P_A(y'_A - y')}{E_{fs}I} \quad , \tag{2.1}$$

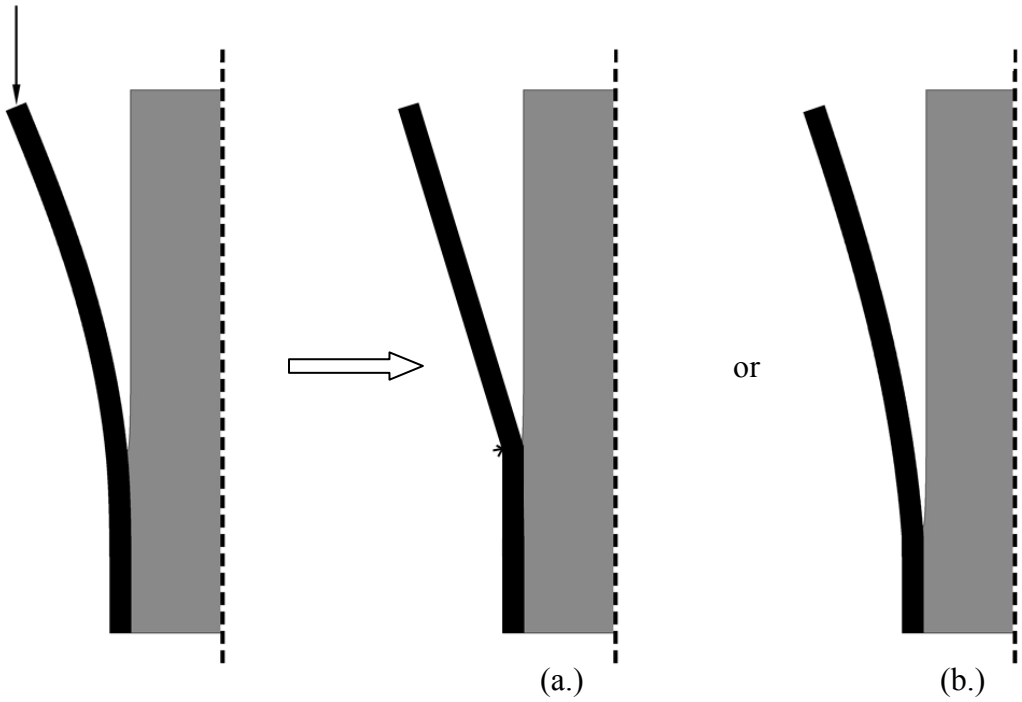

Figure 2.2. Illustration of (a.) facesheet fracture and (b.) core/facesheet debond growth

where M is the bending moment at position s along the beam-column, E_{fs} is Young's Modulus for the facesheet in the x' direction, I is the moment of inertia of the facesheet, P_A is the applied force at A, and y' and y'_A are the y' locations of the beam-column at position s and point A, respectively. Taking the derivative of equation (2.1) with respect to s,

$$\frac{d^2\xi}{ds^2} = -\frac{P_A}{E_{fs}I}\frac{dy'}{ds} \ . \tag{2.2}$$

It is convenient to introduce the constant β for simplification of future expressions, where

$$\beta^2 = -\frac{P_A h^2}{E_{fs}I} \ . \tag{2.3}$$

By acknowledging from Figure 2.1b that $dy'/ds = \sin\xi$, equation (2.2) may be written as

$$\frac{d^2\xi}{ds^2} = -\frac{\beta^2}{h^2}\sin(\xi) \ . \tag{2.4}$$

Through the use of double-angle formulas, this expression may be written as

$$h^2\frac{d}{ds}\left(\frac{d\xi}{ds}\right) = -2\beta^2\sin\left(\frac{\xi}{2}\right)\cos\left(\frac{\xi}{2}\right) \ . \tag{2.5}$$

Both sides of equation (2.5) are now multiplied by $d\xi/ds$ and the entire expression is integrated to yield

$$h^2\left(\frac{d\xi}{ds}\right)^2 = 4\beta^2\left(-\sin^2\left(\frac{\xi}{2}\right)+C_1\right) . \tag{2.6}$$

Variables k and ψ are now introduced such that the constant of integration $C_1 = k^2$, and a change of variables is made such that

$$k\sin(\psi) = \sin\left(\frac{\xi}{2}\right) . \tag{2.7}$$

Thus, equation (2.6) may be written as

$$h^2\left(\frac{d\xi}{ds}\right)^2 = 4\beta^2\left(-\sin^2\frac{\xi}{2}+k^2\right) = 4\beta^2\left(-(k\sin(\psi))^2+k^2\right) . \tag{2.8a}$$

The Pythagorean identity $sin^2\psi + cos^2\psi = 1$ is applied to the rightmost expression in equation (2.8a), and by taking the square root of this expression we obtain

$$\frac{d\xi}{ds} = \frac{2\beta k}{h}\cos(\psi) . \tag{2.8b}$$

We now leave equation (2.8b) in this form and return to equation (2.7). Taking its derivative with respect to s,

$$k\cos(\psi)\frac{d\psi}{ds} = \frac{1}{2}\cos\left(\frac{\xi}{2}\right)\left(\frac{d\xi}{ds}\right) . \tag{2.9a}$$

Solving equation (2.9a) for $d\xi/ds$, the Pythagorean identity is applied and equation (2.7) is substituted to produce

$$\frac{d\xi}{ds} = \frac{2k\cos(\psi)}{\cos\left(\frac{\xi}{2}\right)}\left(\frac{d\psi}{ds}\right) = \frac{2k\cos(\psi)}{\sqrt{1-k^2\sin^2(\psi)}}\frac{d\psi}{ds} \quad . \tag{2.9b}$$

Equations (2.8b) and (2.9b) are both solved for $d\xi/ds$. Equating these expressions and simplifying,

$$\frac{\beta}{h}ds = \frac{d\psi}{\sqrt{1-k^2\sin^2(\psi)}} \quad . \tag{2.10}$$

Integrating equation (2.10) yields

$$\frac{s\beta}{h} = \int_{\psi_B}^{\psi} \frac{d\psi}{\sqrt{1-k^2\sin^2\psi}} = \int_0^{\psi} \frac{d\psi}{\sqrt{1-k^2\sin^2\psi}} - \int_0^{\psi_B} \frac{d\psi}{\sqrt{1-k^2\sin^2\psi}} = F(k,\psi) - F(k,\psi_B) \tag{2.11}$$

where $F(k,\psi)$ is the elliptic integral of the first kind.

Next, the equations describing the shape of the beam-column are found. From Figure 2.1b it is seen that $dx'/ds = \cos\xi$. Through the use of double-angle formulas, dx' can be written in terms of $\xi/2$ as

$$dx' = \left(1 - 2\sin^2\left(\frac{\xi}{2}\right)\right)ds \quad . \tag{2.12a}$$

Equation (2.12a) may be written as

$$dx' = \left(2 - 2\sin^2\left(\frac{\xi}{2}\right)\right)ds - ds = 2\left(1 - \sin^2\left(\frac{\xi}{2}\right)\right)ds - ds \quad . \tag{2.12b}$$

Substituting equation (2.10),

$$dx' = \frac{2h}{\beta}\frac{\left(1-\sin^2\left(\frac{\xi}{2}\right)\right)d\psi}{\sqrt{1-k^2\sin^2(\psi)}} - ds \ . \tag{2.12c}$$

After substituting equation (2.7) into the numerator, equation (2.12c) can be rewritten as

$$dx' = \frac{2h}{\beta}\frac{\left(1-k^2\sin^2(\psi)\right)d\psi}{\sqrt{1-k^2\sin^2(\psi)}} - ds = \sqrt{1-k^2\sin^2(\psi)}d\psi - ds \ . \tag{2.12d}$$

Similarly, from Figure 2.1b it is seen that *dy'/ds = sinξ*. Through the use of double-angle formulas this expression can be written in terms of *ξ/2* as

$$dy' = 2\sin\left(\frac{\xi}{2}\right)\cos\left(\frac{\xi}{2}\right)ds \ . \tag{2.13a}$$

Substituting equation (2.10),

$$dy' = \frac{2h}{\beta}\sin\left(\frac{\xi}{2}\right)\cos\left(\frac{\xi}{2}\right)\frac{d\psi}{\sqrt{1-k^2\sin^2\psi}} \ . \tag{2.13b}$$

Equation (2.7) is substituted for *sin(ξ/2)*, and *cos(ξ/2)* is manipulated through the Pythagorean identity and equation (2.7) such that

$$dy' = \frac{2hk}{\beta}\sin(\psi)\frac{\sqrt{1-k^2\sin^2(\psi)}}{\sqrt{1-k^2\sin^2(\psi)}}d\psi = \frac{2hk}{\beta}\sin(\psi)d\psi \ . \tag{2.13c}$$

Integrating equations (2.12d) and (2.13c), we have

$$x' = \frac{2h}{\beta}\int_{\psi_B}^{\psi}\sqrt{1-k^2\sin^2(\psi)}\,d\psi - s = \frac{2h}{\beta}\left(E(k,\psi)-E(k,\psi_B)\right)-s \tag{2.14a}$$

and

$$y' = \frac{2hk}{\beta}\int_{\psi_B}^{\psi}\sin(\psi)\,d\psi = \frac{2hk}{\beta}\left(\cos(\psi)-\cos(\psi_B)\right) \tag{2.14b}$$

where $E(k,\psi)$ is the elliptic integral of the second kind.

Application of Boundary Conditions

Now that the general equations have been developed it is possible to analyze the beam-column shown in Figure 2.1b. The following approach follows a similar progression to that of Aristizabal-Ochoa [2].

First, boundary conditions at point *A* (tip of the facesheet) are specified. It is first recognized that at point *A* (where $s=h$) $M_A = 0$. Substituting into equation (2.1), $(d\xi/ds)_A = 0$. Substituting into equation (2.8b),

$$0 = \frac{2\beta k}{h}\cos(\psi_A) \ . \tag{2.15}$$

Recognizing that β, k, and h are all nonzero to avoid a trivial solution, it is found that $\psi_A=\pi/2$. Applying equation (2.7) at point *A* and solving for k,

$$k = \sin\left(\frac{\xi_A}{2}\right) . \tag{2.16}$$

Applying equation (2.11) at point *A*,

$$\beta = \int_{\psi_B}^{\psi_A} \frac{d\psi}{\sqrt{1-k^2\sin^2\psi}} = F(k,\psi_A) - F(k,\psi_B) \ . \tag{2.17}$$

Similarly, equations (2.14a) and (2.14b) can be evaluated at point *A* as

$$x'_A = \frac{2h}{\beta}\left(E(k,\psi_A) - E(k,\psi_B)\right) - h \tag{2.18}$$

and

$$y'_A = \frac{-2hk}{\beta}\left(\cos(\psi_A) - \cos(\psi_B)\right) = \frac{2hk}{\beta}\cos(\psi_B) \ . \tag{2.19}$$

The expression for rotation ξ_B at the crack tip (s=0) is defined as

$$\xi_B = \frac{M_B}{\kappa_B} = \frac{-P_A y'_A}{\kappa_B} \ . \tag{2.20}$$

Substituting this into equation (2.7),

$$k\sin(\psi_B) = \sin\left(\frac{-P_A y'_A}{2\kappa_B}\right) \ . \tag{2.21}$$

Equating equations (2.1) and (2.8b) at point *B* with $M_B = -P_A y'_A$, we have

$$\left(\frac{d\xi}{ds}\right)_B = \frac{P_A y'_A}{E_{fs} I} = \frac{2\beta k}{h}\cos(\psi_B) \ . \tag{2.22}$$

For a given set of values for E_{fs}, I, κ_B, and h, from the equations listed in the previous section there exists a set of four nonlinear equations with five unknowns: β, P_A, y'_A, ψ_B and k.

$$k = \frac{\sin\left(\frac{-P_A y'_A}{2\kappa_B}\right)}{\sin(\psi_B)} \tag{2.23}$$

$$\beta = F(k,\psi_A) - F(k,\psi_B) \tag{2.24}$$

$$P_A = -\frac{\beta^2 E_{fs} I}{h^2} \tag{2.25}$$

$$y'_A = \frac{2hk}{\beta}\cos(\psi_B) \tag{2.26}$$

By substituting the expressions for P_A and β into the other equations the problem is reduced to 2 equations and 3 unknowns. These equations, presented below, must be solved in order to describe the system's forces and deflections.

$$k = \frac{\sin\left(\frac{\left(F(k,\psi_A) - F(k,\psi_B)\right)^2 E_{fs} I y'_A}{2h^2\kappa_B}\right)}{\sin(\psi_B)} \tag{2.27}$$

$$y'_A = \frac{2hk\cos(\psi_B)}{F(k,\psi_A) - F(k,\psi_B)} \tag{2.28}$$

Determining Values for κ_B

Using the two nonlinear equations (2.27) and (2.28) and specified values for E_{fs}, I, h, and κ_B, G_I (defined as the Mode I strain energy release rate) and facesheet stresses can be calculated. Whereas h is specified and E_{fs} and I are known for a given facesheet material and geometry, κ_B is not a fundamental material property of the core or facesheet alone and thus requires calculation. It can be seen from Figure 2.1 that the torsional spring with stiffness κ_B at the crack tip is used in place of all core material as well as the facesheet in the bonded region of the sandwich composite. Thus the value of κ_B depends on both core and facesheet properties, and each sandwich will have a unique κ_B value.

To determine κ_B values, the sandwich composite was treated as a Beam On an Elastic Foundation (BOEF). Figure 2.3 shows how the BOEF approach is utilized.

From Figure 2.3 it can be seen that the resultant shear force at the crack tip from force P_A is unaccounted for and thus only its resultant bending moment M_B at the crack tip is accounted for. Following the derivation of Cook and Young [3] the slope along the length of the beam may be expressed as

$$\theta = \frac{4\zeta^3 M_B}{k_o b} D_{\zeta x} \ , \tag{2.29}$$

where

$$D_{\zeta x} = e^{-\zeta x} \cos(\zeta x) \ , \tag{2.30}$$

$$\zeta = \left(\frac{k_o b}{4 E_{fs} I} \right)^{1/4} \ , \tag{2.31}$$

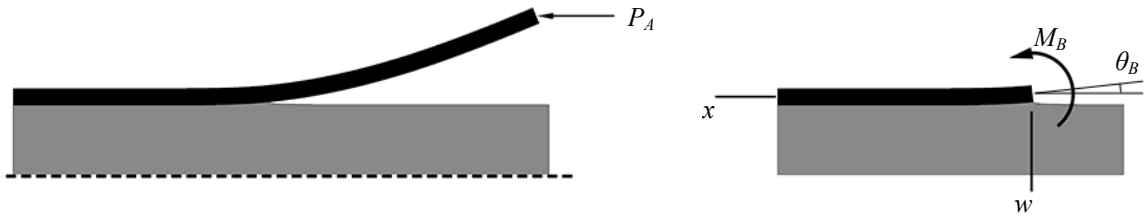

Figure 2.3. Adaptation of a general sandwich composite (a.) to a Beam on Elastic Foundation (b.)

$$k_o = \frac{E_c}{t_c/2} \ , \tag{2.32}$$

$$I = \frac{t_{fs}{}^3 b}{12} \ , \tag{2.33}$$

and b is specimen width.

Evaluating equation (2.29) at the crack tip B (x=0),

$$\kappa_B = \frac{M_B}{\theta_B} = \frac{k_o b}{4\zeta^3} = \frac{E_c b}{4\left(\frac{t_c}{2}\right)\zeta^3} \ . \tag{2.34}$$

Thus, the BOEF method yields a simplified expression for κ_B. For a given sandwich composite equation (2.34) can be evaluated and used in equation (2.27).

Using MATLAB to Solve Analytical Model

Solutions of the two nonlinear equations for a specific sandwich configuration were obtained through the use of MATLAB [4]. The following describes the basic steps and iterations used to generate plots designers can use to design sandwich composites for increased energy absorption.

Calculation of G_I

The mode I strain energy release rate G_I is defined as

$$G_I = -\frac{1}{b}\frac{dU}{dh} \ , \tag{2.35}$$

where U is the total strain energy, b is specimen width and h is crack length. The derivative dU/dh is approximated with $\Delta U/\Delta h$ over a small spacing, and equation (2.35) may be written as

$$G_I = -\frac{1}{b}\frac{\Delta U}{\Delta h} \ . \tag{2.36}$$

Thus, G_I can be calculated as shown in Figure 2.4 by comparing energy states 1 and 3 representative of the crack just before and after crack growth, respectively.

Energy state 1 in Figure 2.4 corresponds to the deformed state of a given sandwich composite at the instant that G_I reaches G_{Ic}, just before crack growth. In a displacement-driven test it is assumed that there is no change in *x'*-deflection during crack growth, such that just after crack growth energy state 3 is reached. Energy state 2 is a nonphysical intermediate step used in finding energy state 3, and will be discussed in a later section. Once energy states at 1 and 3 are known G_I can be calculated from equation (2.36) as

$$G_I = \frac{\left(U_1 - U_3\right)}{b\Delta h} \ . \tag{2.37}$$

The method used for calculation of energy states 1 through 3 is discussed in the following section.

Steps Used in MATLAB to Solve Analytical Model

The steps outlined in the following section describe the iterative approach utilized to solve the analytical model and create plots which can be used to design for increased

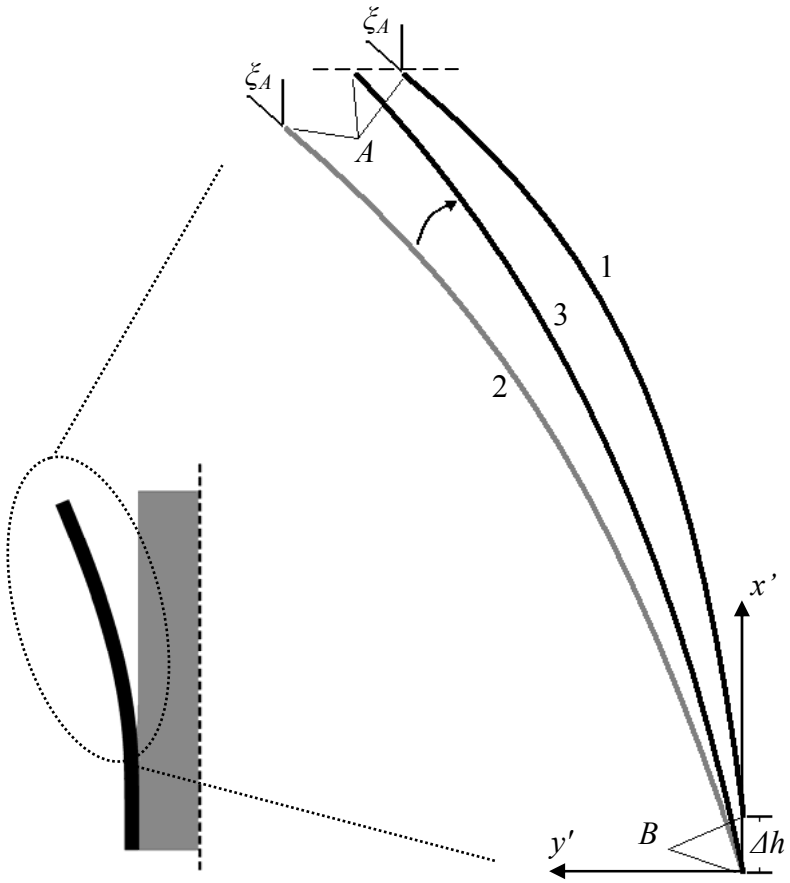

Figure 2.4. Depiction of three energy states used in MATLAB Solution of analytical model

energy absorption. The general MATLAB procedure is shown in Figure 2.5 and discussed in detail in the following paragraphs.

Step 0 – Specify material properties and sandwich geometry

In order to solve the analytical model, values must be prescribed for specimen width b, facesheet thickness t_{fs}, facesheet modulus of elasticity E_{fs}, core thickness t_c, core modulus of elasticity E_c, mode I critical strain energy release rate G_{Ic}, allowable facesheet stress $\sigma_{fs,allowable}$, crack length h and the appropriate value for κ_B as described previously.

Step 1 – Give an initial guess for ξ_A

As stated previously, the shape of the facesheet is described by two nonlinear equations with three unknowns. In order to solve this set of equations one of the variables must be known – or specified. In this case it makes sense to specify a value for an unknown that carries physical meaning – specifically, either y'_A (facesheet tip outward deflection) or k (calculated by specification of facesheet tip angle ξ_A where $k = sin(\xi_A/2)$ as defined previously). In this case it was chosen to specify ξ_A, although specifying either of the two would result in a solvable set of equations. Ideally one would specify the value for ξ_A whose corresponding $G_I = G_{Ic}$; however, since this state is unknown an iterative approach is necessary. To begin the iterative process, a value of ξ_A should be selected such that the calculated value of G_I will be significantly lower than G_{Ic}.

Step 2 – Solve the nonlinear equations and find Strain Energy U_1

With ξ_A specified the deflected facesheet shape is now described by two equations with two unknowns and can be solved using MATLAB's fsolve command. It is important to note that elliptic integrals are evaluated numerically by breaking the function

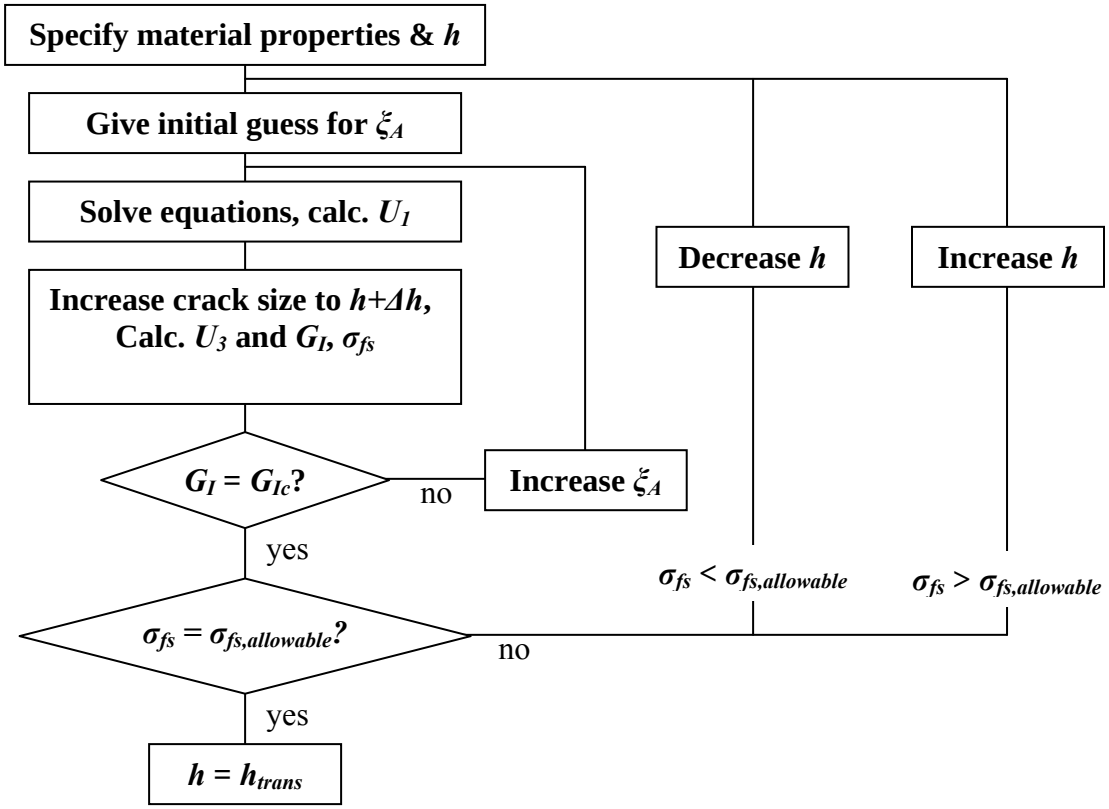

Figure 2.5. Flow chart outlining general MATLAB procedure

into n discrete bins and performing a trapezoidal integration. After solving for the unknowns the value of s (Equation 2.11) and bending moment are then calculated at each of these discrete points, and the strain energy for each bin is calculated and summed to find U_1 as

$$U_1 = \frac{1}{2E_{fs}I} \cdot \sum_{n=2}^{n} \left(\frac{\left(M_n^2 + M_{n-1}^2\right)}{2} \left(s_n - s_{n-1}\right) \right) . \tag{2.38}$$

Step 3 – Increase crack length by Δh and calculate U_3

Energy U_3 is calculated by first increasing the crack size a small amount from h to $h+\Delta h$. The tip angle is taken as ξ_A from step 1 and step 2 is then repeated, resulting in energy state 2 shown in Figure 2.4. It is apparent from Figure 2.4 that the tip deflection in the x' direction is larger than for energy state 1, thus an iterative procedure is then taken where the tip angle ξ_A is repeatedly decreased until energy state 3 is reached, where $x'_{A,1} + \Delta h = x'_{A,3}$. G_I is then calculated using equation (2.37) and compared to G_{Ic}. If $G_I < G_{Ic}$, a slightly larger ξ_A value is chosen in step 1 and the process is repeated until the resulting $G_I = G_{Ic}$.

Step 4 – Calculate σ_{fs}

Once the conditions for $G_I = G_{Ic}$ have been met, it is necessary to calculate the stress in the facesheet. Stresses in the facesheet are a combination of bending and compressive stresses, and the location of the largest stress in the facesheet is at the outer surface of the facesheet and at the cross section located at the crack tip. The compressive axial stress and compressive bending stress combine at this point to produce a maximum facesheet stress of

$$\sigma_{fs} = \frac{P_A}{t_{fs} b} - \frac{M_B \frac{t_{fs}}{2}}{I} \quad . \tag{2.39}$$

If the calculated stress value differs from the allowable facesheet stress $\sigma_{fs,allowable}$ the crack length is changed and the entire process is repeated until $\sigma_{fs} = \sigma_{fs,allowable}$. The corresponding crack length represents the "transition crack length" (h_{trans}), where G_I reaches G_{Ic} and σ_{fs} reaches $\sigma_{fs,allowable}$ simultaneously. Below this crack length the facesheets are predicted to fail in bending before further crack growth can occur and increased energy absorption is expected. Conversely, larger cracks are predicted to experience continual crack growth until total core/facesheet debond or an external constraint is reached. Thus, a sandwich design with a high h_{trans} value would be deemed more crashworthy than one with a low h_{trans} value.

Materials

Description of Sandwich Parameter Variations

In order to create the plots mentioned previously it was necessary to define a realistic range for each of the material properties and facesheet/core geometries to be considered in the model. It was also necessary to define a "baseline" value for each parameter that would be used while varying other material properties and geometries.

Facesheet thickness (t_{fs})

Facesheet thicknesses used in the study ranged from 0.5-3.0 mm (0.02-0.12 in.). This represents a realistic range for use in sandwich composites when paired with the

other material property/geometry ranges described below. The "baseline" value used was 1.0 mm.

Facesheet modulus (E_{fs})

Due to the wide variety of facesheet materials that could be used in sandwich construction it was necessary to include a wide variety of facesheet modulus values in the study. However, the other material property/geometry ranges discussed in this section limited the range of possible facesheet values; thus, facesheet modulus values used in the study ranged from 25-50 GPa, with the lower and upper limits representative of a typical quasi-isotropic E-glass/epoxy facesheet and a typical quasi-isotropic carbon/epoxy facesheet, respectively. When paired with the other material properties and geometries described in this section, 25 GPa and 50 GPa represent the upper and lower limits of model functionality, respectively. Facesheet moduli below 25 GPa result in beam-columns that may fail in compression before buckling occurs for some facesheet thicknesses, whereas facesheet moduli above 50 GPa may reach tip angles ξ_A greater than 90° for thin facesheet thicknesses. The "baseline" value for facesheet modulus was 50 GPa.

Core thickness (t_c)

The typical role of the core material in sandwich composite application is to carry shear loads and to separate the facesheets in order to increase the bending stiffness of the plate without adding significant weight. Common core thicknesses range anywhere from a few millimeters up to several centimeters; for this study core thickness was varied from

3.175-25.4 mm (0.125-1.0 in.). The "baseline" value used in the study was 12.7 mm (0.5 in.).

Core modulus (E_c)

As with facesheet modulus, core modulus is another sandwich property where a large range was necessary due to the wide variety of core materials available. The range of core modulus values used in the study was 50-1000 MPa, representative of materials ranging from low-density polyurethane foam to aluminum honeycomb. The "baseline" value used in the study was 500 MPa, typical of a Nomex honeycomb.

Mode I critical strain energy release rate (G_{Ic})

Values for G_{Ic} are highly dependant on the facesheet and core materials used. For this reason a wide range of values was chosen for G_{Ic}, from 175-1000 J/m^2. In the realm of typical sandwich composites, this range incorporates both "weak" and "strong" interfaces. The "baseline" value used in this study was 500 J/m^2.

Other Sandwich Properties/Geometries

The following additional material properties and sandwich geometries were used in the solution of the analytical model: facesheet allowable stress $\sigma_{fs,allowable}$ = 600 MPa, specimen width b = 25.4 mm (1.0 in.), and Δh = 0.25 mm.

Analytical Model Results

Solutions obtained through the methods described previously are presented in the following sections. The plots shown in the following sections were made by solving the analytical model for h_{trans} while varying numerous different pairs of material

properties/sandwich geometries (such as core modulus and core thickness) using "baseline" values for all other material properties and sandwich geometries. Golden Software Surfer 7 [5] was used to transform the resulting 3-D table into a 2-D contour plot displaying lines of constant h_{trans}.

Core Design 1 (varying E_c and t_c)

The results obtained by varying core modulus (E_c) and core thickness (t_c) are shown in Figure 2.6. Figure 2.6 shows that the transition crack length h_{trans} increases with decreasing core modulus and increasing core thickness. For the range of core modulus and core thicknesses studied, h_{trans} ranges from approximately 10-24 mm (0.39-0.94 in.). It can be seen in Figure 2.4 that a core modulus of 200 MPa and core thickness of 10 mm yields an h_{trans} value of approximately 15 mm. Thus, a sandwich with these specific property and geometry values is predicted to experience facesheet fracture with any core/facesheet debond smaller than 15 mm, whereas a debond larger than 15 mm is expected to experience core/facesheet debond growth.

A contour plot of h_{trans} as a function of core modulus E_c and core thickness t_c could be useful as a general tool for designers. If given a facesheet material and a choice of potential core materials, a designer could generate a contour plot of h_{trans} as a function of core modulus E_c and core thickness t_c to determine the most suitable core for their specific energy absorption or failure mode requirements. The plot could also be used to determine how sensitive a core material might be to variability in the core Young's Modulus or core thickness. It can be seen from Figure 2.6 that for a high core modulus and low core thickness (lower-right quadrant of plot) a significant change in core

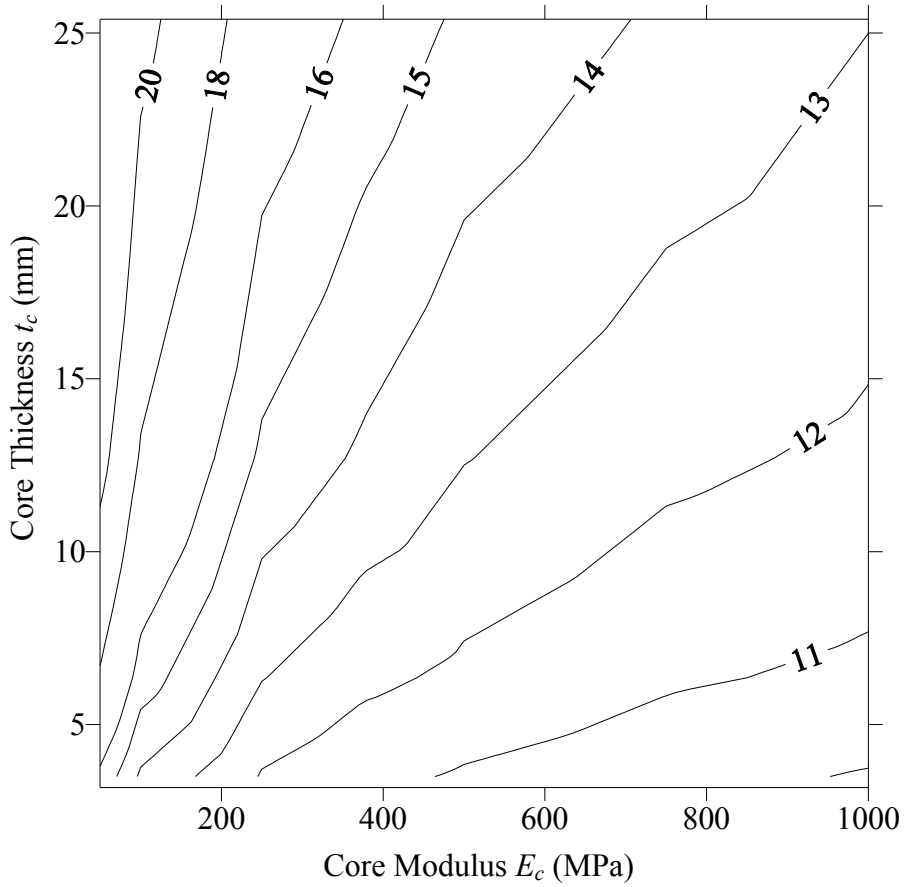

Figure 2.6. Plot of h_{trans} as a function of E_c and t_c

modulus or core thickness yields only a small change in h_{trans}. Alternately, for low core modulus and large core thickness (upper-left quadrant of plot) a small change in core modulus or core thickness yields a significant change in h_{trans}, suggesting that candidate cores lying within this area of the plot are more sensitive to variability in stated core modulus and thickness.

Core Design 2 (varying G_{Ic} and t_c)

The results obtained by varying mode I critical strain energy release rate (G_{Ic}) and core thickness (t_c) are shown in Figure 2.7. From Figure 2.7 it can be seen that the transition crack length h_{trans} increases with increasing critical strain energy release rate and increasing core thickness. For the range of G_{Ic} and core thicknesses studied, h_{trans} ranges from approximately 5-80 mm (0.20-3.15 in.). The plot suggests that h_{trans} is highly dependent on G_{Ic}; a small change in G_{Ic} produces a significant change in h_{trans}. This is due to the squared relationship between applied load and strain energy seen in equation (2.38), where a small increase in applied load P_A yields a large change in strain energy and thus a large change in the calculated G_I value.

A contour plot of h_{trans} as a function of mode I critical strain energy release rate G_{Ic} and core thickness t_c could be used by a designer to help choose facesheet/core combinations. If the goal is to prevent core/facesheet debonding it is apparent that one would want to choose the combination with a high G_{Ic} or a low $\sigma_{fs,allowable}$ such that the facesheet is likely to fail before crack growth occurs. Due to the large sensitivity of G_{Ic} to bond quality, it is apparent from Figure 2.7 that steps must be taken in the manufacturing stage of sandwich composites to create consistent, high quality bonds or else the sandwich may become more vulnerable to crack growth.

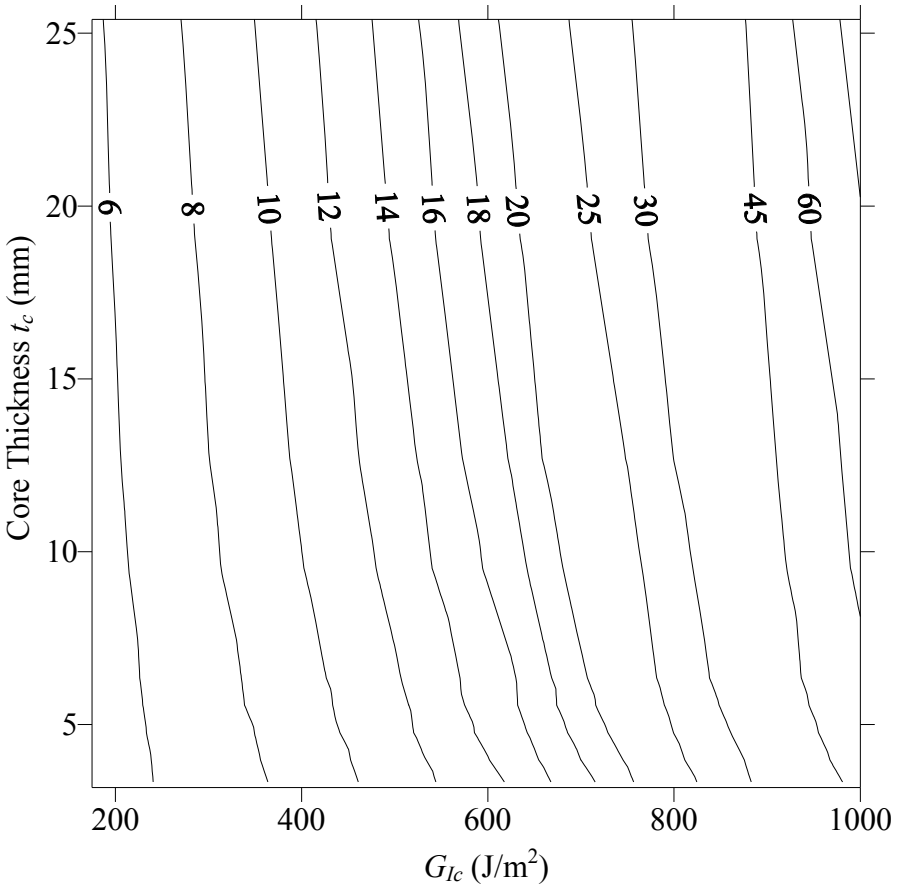

Figure 2.7. Plot of h_{trans} as a function of G_{Ic} and t_c

Facesheet Design (varying E_{fs} and t_{fs})

The results obtained by varying facesheet modulus (E_{fs}) and facesheet thickness (t_{fs}) are shown in Figure 2.8. For the range of facesheet modulus and facesheet thickness values used h_{trans} ranges from approximately 5-40 mm (0.2-1.6 in.). The general trend seen in Figure 2.8 is quite different from the trends seen in Figures 2.6 and 2.7. The plot shows that h_{trans} increases with increasing facesheet modulus E_{fs}. However, h_{trans} first decreases then *increases* with increasing facesheet thickness t_{fs}. This trend was not seen in the other two plots (Figures 2.6 and 2.7), where h_{trans} tended to either increase or decrease continually with increasing core properties.

The reason for the decrease then increase in h_{trans} with increasing facesheet thickness is illustrated in Figure 2.9. As seen in Figure 2.9, at short crack lengths there is a higher level of facesheet stress at crack growth for thicker facesheets. However, at long crack lengths the facesheet stress at crack growth is higher for thin facesheets. The value for $\sigma_{fs,allowable}$ used in obtaining Figure 2.8 was 600 MPa, which lies in the region of facesheet stress where this change is occurring; this may be a contributor to the trend seen in Figure 2.8.

Another possible contributor to the trend seen in Figure 2.8 is the nature of the stresses corresponding to extreme thin and thick facesheets. Thin facesheets tend to have a relatively large deflection at h_{trans} such that bending stresses due to M_B are large even though the applied load P_A and thus axial stresses are small. As facesheet thickness increases, the force required for buckling increases such that P_A and the axial stresses increase while M_B and bending stresses decrease due to the reduced deflection. The relative rates of these changes may contribute to the trends seen in Figure 2.8.

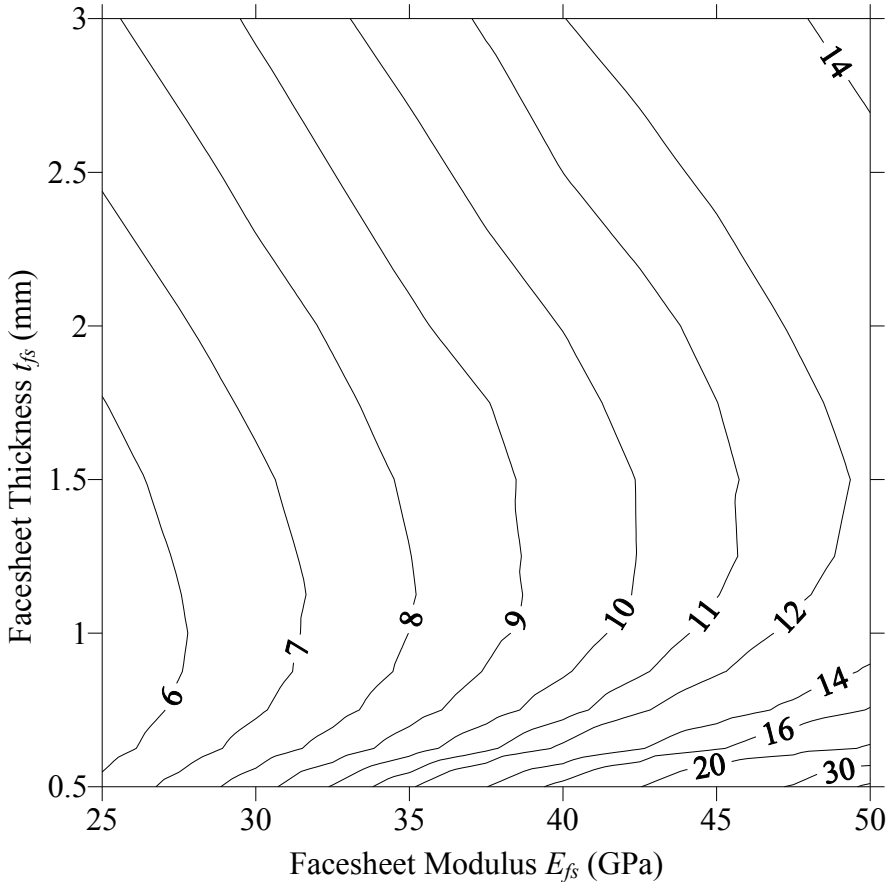

Figure 2.8. Plot of h_{trans} as a function of E_{fs} and t_{fs}

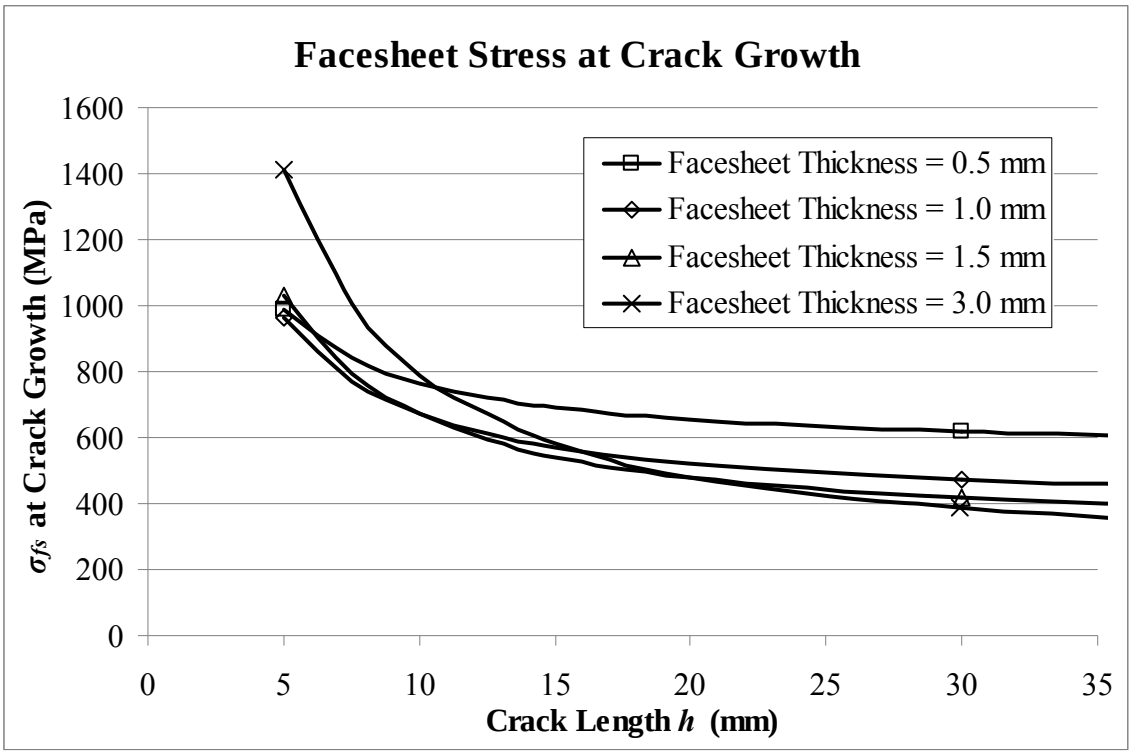

Figure 2.9. Facesheet stress versus crack length for variation of facesheet thickness

A plot of h_{trans} as a function of facesheet modulus E_{fs} and facesheet thickness t_{fs} could be used by a designer in several ways. If given a core material and a choice of potential facesheet materials, a designer could generate a plot of h_{trans} as a function of facesheet modulus E_{fs} and facesheet thickness t_{fs} to determine the most suitable core for their specific energy absorption or failure mode requirements.

Using ANSYS to Validate κ_B Calculation Method

In order to validate the elastic foundation values used for κ_B, a 2-D geometrically nonlinear finite element analysis was performed using ANSYS 11 with PLANE42 elements [6]. Figure 2.10 shows a typical ANSYS mesh used in the study. Due to the buckling nature of the problem, a force-driven approach was not feasible and instead x and y-displacements were applied at the tip of the facesheet along the centerline; this effectively served to prevent buckling and allow the model to reach an equilibrium solution. In order to compare κ_B values, the facesheet tip x-displacement used in the finite element model was set equal to the x-displacement value at crack growth from the analytical model. The finite element model was then iterated with varying y-displacement values until the resulting facesheet tip outward force F_Y was 0, thus matching the loading scheme used in the analytical model (Figure 2.1).

Materials Used in ANSYS Model

Material properties used in the model validation investigation are shown in Table 2.1 with coordinate directions consistent with Figure 2.10. The facesheet material properties used in the study are representative of a T300B 3K plain weave carbon fabric

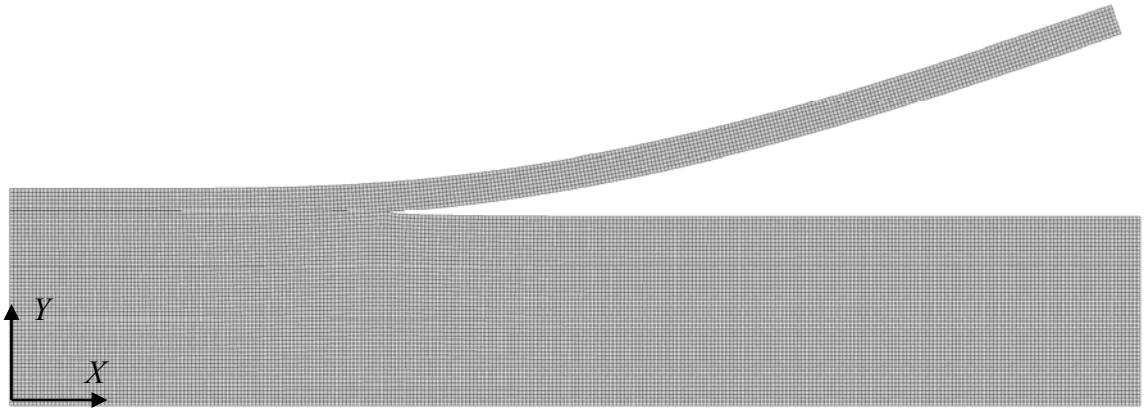

Figure 2.10. Representation of a typical mesh used in ANSYS

Table 2.1. Material properties used with ANSYS

Material	Property	Value (SI)	Value (ENG)
Facesheet	E_x	30.8 GPa	4.47 Msi
	E_y	10.6 GPa	1.54 Msi
	E_z	30.8 GPa	4.47 Msi
	ν_{xy}	0.26	0.26
	ν_{xz}	0.35	0.35
	ν_{yz}	0.26	0.26
	G_{xz}	3.86 GPa	0.56 Msi
	G_{xy}	4.14 GPa	0.60 Msi
Core - Balsa	E_x	42.5 MPa	6.16 ksi
	E_y	322 MPa	46.7 ksi
	E_z	42.5 MPa	6.16 ksi
	ν_{xy}	0.01	0.01
	ν_{xz}	0.34	0.34
	ν_{yz}	0.34	0.34
	G_{xy}	120 MPa	17.4 ksi
Core - Polyurethane	E (isotropic)	86.2 MPa	12.5 ksi
	ν (isotropic)	0.30	0.30

(referred to as WC subsequently) oriented in a quasi-isotropic ($[(0/90)/(\pm45)]_{nT}$) layup (where n=1, 2, or 3) and infiltrated with a matrix comprised of EPON 862 epoxy resin and EPON 9553 hardener. The core materials included polyurethane foam and end-grain balsa wood (referred to subsequently as PU and B, respectively). The polyurethane foam properties are representative of Last-A-Foam FR-6710, with a density of 160 kg/m^3 supplied by General Plastics Manufacturing Company. The end-grain balsa wood properties are representative of SuperLite S67, with a density of 112 kg/m^3 supplied by Baltek Corporation.

κ_B Calculation Method

Following the solution of the finite element model, κ_B was calculated using applied forces and crack tip deflections. Figure 2.11 illustrates the calculation of the angle of rotation of the facesheet at the crack tip. Using nodes 1 and 2 originally separated by node spacing S_o, the facesheet rotation angle θ was found from trigonometry as

$$\theta = \tan^{-1}\left(\frac{u_{2,y} - u_{1,y}}{S_o + u_{2,x} - u_{1,x}}\right) . \tag{2.34}$$

Referring to Figure 2.12, the bending moment at the crack tip was calculated as

$$M_{cracktip} = F_x(u_{fs,y} - u_{cracktip,y}) . \tag{2.35}$$

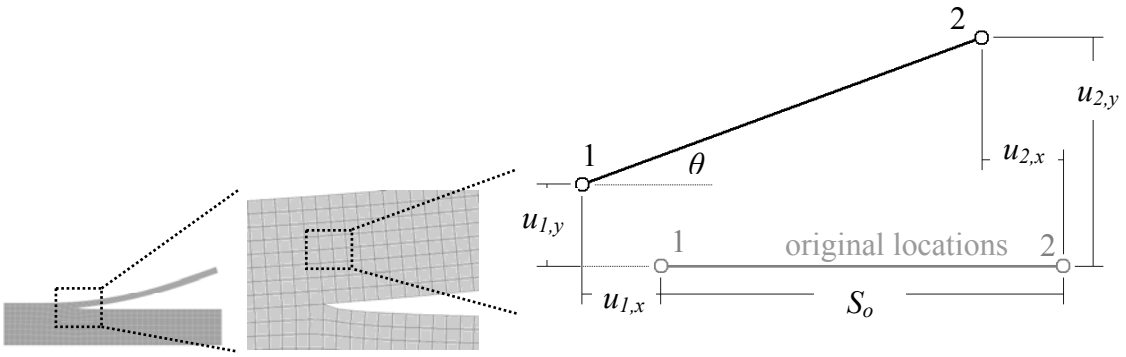

Figure 2.11. Progressive zooming of mesh showing dimensions used in calculation

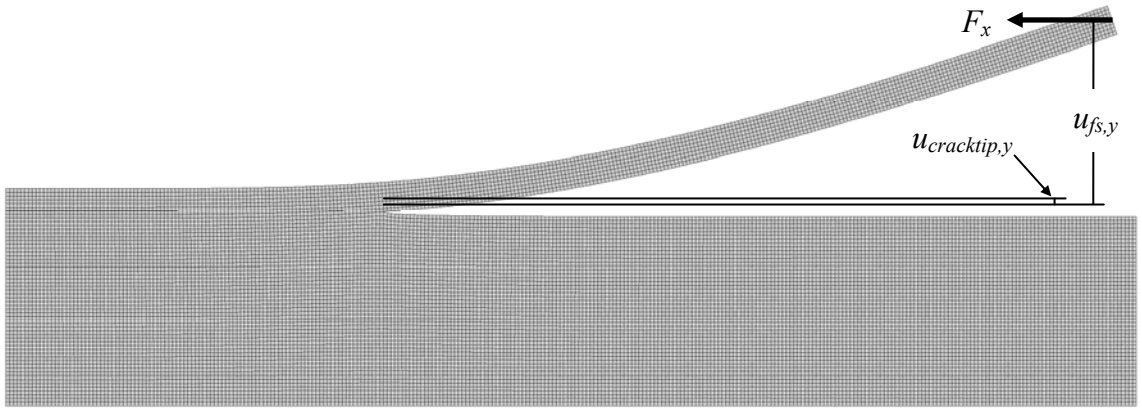

Figure 2.12. Finite element mesh showing dimensions for calculation of $M_{cracktip}$

After finding θ and $M_{cracktip}$, the value for κ_B was calculated as $\kappa_B = M_{cracktip} / \theta$. This value could then be compared against the values found using the Beam on Elastic Foundation method discussed previously.

Finite Element Analysis Results

Table 2.2 compares κ_B values obtained from the Beam On Elastic Foundation (BOEF) and finite element analyses for varying thicknesses of the woven carbon facesheets with each core material. The BOEF calculated value for κ_B is lower than the finite element calculation for each of the sandwich configurations tested, with the difference increasing with decreasing facesheet thickness. This trend is expected, as all core material within the debonded region is neglected in elastic foundation calculations. In reality the debonded core material near the crack tip is displaced outward, thus providing resistance to rotation.

Because the percent differences from Table 2.2 are significant, a sensitivity study was performed to determine the analytical model sensitivity to κ_B values. Increasing κ_B by 25% and 50% in the analytical model using "baseline" values yielded 11.3% and 20.5% decreases in h_{trans}, respectively, which is significant and suggests that an alteration to the BOEF method of calculating κ_B may be necessary. However, it is expected that this decrease in h_{trans} will occur for all sandwich configurations such that the trends seen in Figures 2.6-2.8 would be consistent with those observed using updated κ_B values.

Summary and Conclusions

Designing sandwich composites for energy absorption under edgewise compression loading requires the sandwich to be tailored towards high energy-absorbing

Table 2.2. Comparison of ANSYS and BOEF calculations for κ_B

Sandwich Configuration	κ_B (N-m/rad)		
	ANSYS	BOEF	% Difference
6-ply WC-PU	37.72	32.09	-14.92
4-ply WC-PU	17.33	12.89	-25.61
2-ply WC-PU	4.25	2.71	-36.23
6-ply WC-B	55.61	44.62	-19.76
4-ply WC-B	24.56	17.92	-27.03
2-ply WC-B	6.02	3.77	-37.45

failure modes. For sandwich composites with a preexisting core/facesheet debond, two competing failure modes exist: facesheet fracture and core/facesheet debond growth. A given sandwich configuration can be analyzed through the use of an analytical model in order to determine the "transition crack length", h_{trans}. Below this crack length the facesheets are predicted to fail in bending before further crack growth can occur and increased energy absorption is expected. Conversely, larger cracks are predicted to experience continual crack growth until total core/facesheet debond or an external constraint is reached. Thus, a sandwich design with a high h_{trans} value would be deemed more crashworthy than one with a low h_{trans} value.

By varying pairs of core or facesheet properties/geometries, plots were constructed showing the variation of h_{trans} with these parameters. Results showed that h_{trans} increased with decreasing core modulus and increasing core thickness. Transition crack length h_{trans} was found to be highly sensitive to bond strength, where a small increase in G_{Ic} yielded a significant increase in h_{trans}. A varying trend was seen with facesheet thickness, where h_{trans} first decreased then increased with increasing facesheet thickness; this is believed to be due to the changing nature of the stresses for the specific range of properties used in this study. A finite element analysis showed that the Beam On Elastic Foundation method underpredicted κ_B values, which suggest that a change in calculation method may be necessary.

Contour plots of h_{trans} as a function of two varying properties/geometries could be useful as a tool for a designer in several ways. If given a facesheet material and several candidate core materials, a designer could generate a contour plot similar to those presented in this paper. Candidate core materials could then be compared against each

other to find the core with the largest h_{trans} value; this core material would then be deemed the most crashworthy. At this stage the designer could also take into account variables such as weight or material and manufacturing costs such that the tool becomes customized to their specific design problem.

A contour plot such as those presented in this paper could also be used to investigate the sensitivity of a given sandwich composite to variability in a specific property/geometry. For example, if significant variability in a core material's Young's Modulus is possible (as is inherent in end-grain balsa wood), a contour plot which varies core Young's Modulus could be created. From this plot the change in h_{trans} with core Young's Modulus could be determined and the sandwich could be analyzed for any added susceptibility to core/facesheet debond growth due to this variability.

A sandwich composite with prior damage or manufacturing error resulting in a core/facesheet debond could be analyzed using contour plots such as those presented in this paper. Using the sandwich's specific properties as input, the model presented in this paper could be solved and the value of h_{trans} for the sandwich could be calculated. This number could then be compared to the length of the sandwich's existing debond. If h_{trans} is approximately equal to or smaller than the existing debond length, the sandwich is at high risk of experiencing core/facesheet debond growth and low energy absorption during a subsequent impact event. This would suggest that the sandwich should be either repaired or replaced such that core/facesheet debond growth is prevented and maximum energy absorption is achieved.

Notation

The following symbols are used in this paper:

b = sandwich composite width;

E_c = modulus of elasticity of core material;

E_{fs} = modulus of elasticity in x'-direction of facesheet material;

G_I and G_{Ic} = strain energy release rate and critical strain energy release rate, respectively;

h = crack length;

h_{trans} = transition crack length, crack length at which G_I=G_{Ic} and $\sigma_{fs} = \sigma_{fs,\ allowable}$ simultaneously;

I = principal moment of inertia of the beam-column;

M = bending moment at any point s along the length of the beam-column;

P_A = force applied at point A along the centerline of the beam-column;

t_c = core thickness;

t_{fs} = facesheet thickness;

U = strain energy stored within the beam-column;

x'_A and y'_A = displacements of point A in the x' and y' directions, respectively;

κ_B = stiffness of the torsional spring at point B;

σ_{fs} = Maximum stress (compressive) in beam-column at point $B = P_A/(t_{fs}b) - M_B(t_{fs}/2)/I$;

$\sigma_{fs,\ allowable}$ = Maximum allowable stress in beam-column before

failure occurs; and

ξ, ξ_A, and ξ_B = angle between *x'* axis and tangent to beam-column at *s*, point *A*, and point *B*, respectively;

References

1. Van Otten J, Stapleton SE, Adams DO. Design considerations for energy absorption in automotive sandwich composites. Paper presented at: ISTC 2008. Proceedings of the 40th International SAMPE Technical Conference, 2008 Sep 8-11; Memphis, TN.

2. Aristizabal-Ochoa JD. Large deflection stability of slender beam-columns with semirigid connections: elastica approach. J Eng Mech. 2004; 130(3):274-282.

3. Cook RD, Young WC. Beams on an elastic foundation. In: Advanced mechanics of materials 2nd edition. Upper Saddle River NJ: Prentice Hall, 1999; p. 133-160.

4. MATLAB [computer program]. Version 7.7. Natick (MA): MathWorks; 2008.

5. Surfer [computer program]. Version 7.04. Golden (CO): Golden Software, Inc.; 2001.

6. ANSYS [computer program]. Version 11.0. Canonsburg (PA): ANSYS, Inc.; 2007.